JOURNAL OF GUIDANCE, CONTROL, AND DYNAMICS
Vol. 32, No. 4, July–August 2009

Computation and Applications of an Orbital Dynamics Symplectic State Transition Matrix

Yuichi Tsuda*
Japan Aerospace Exploration Agency, Kanagawa 229-8510, Japan
and
Daniel J. Scheeres†
University of Colorado at Boulder, Boulder, Colorado 80309-0429

DOI: 10.2514/1.42358

This paper presents a numerical method for deriving a symplectic state transition matrix for an arbitrary Hamiltonian dynamical system. It provides the exact solution-space mapping of the linearized Hamiltonian systems, preserving the symplectic structure that all Hamiltonian systems should possess by nature. The symplectic state transition matrix can be applied to accurate, yet computationally efficient, dynamic filters, long-term propagations of the motions of formation-flying spacecraft, eigenstructure/manifold analysis of *N*-body dynamics, etc., when the exact structure-preserving property is crucial. We present the derivation and key characteristics of the symplectic state transition matrix and apply it to the two-body dynamics, the circular restricted three-body problem, and an Earth orbit with perturbation forces based on the real ephemeris. These numerical examples reveal that this numerical symplectic state transition matrix shows improvements in preserving the structural properties of the state transition matrix as compared with the conventional linear state transition matrix with Euler or Runge–Kutta integrations.

I. Introduction

THE symplectic property is a fundamental geometrical structure of any Hamiltonian system. Many important features of Hamiltonian systems, such as energy and momentum preservation, manifold structures, and eigenstructures, are strongly related to the symplectic property. Such geometrical structures can be contained and preserved in the numerical solutions if this symplectic property is properly implemented in the numerical method of solving the Hamiltonian systems. Indeed, there are already many studies on symplectic integrators, which solve ordinary differential equations while preserving the symplectic structure.

On the other hand, the linearization of the dynamical systems is an important mathematical tool for engineering analysis. It is sometimes understood as a simplification at the cost of losing precision, especially in the context of numerical simulations studies. The truth, of course, is more than that. Many current guidance, navigation, and control techniques, such as dynamic filters, robust control logic, etc., rely on linearized formulations, and even more fundamental studies of nonlinear systems, such as manifolds and eigenstructures, are also studied using linearizations.

This paper proposes a solution-space mapping scheme for linearized Hamiltonian systems that exactly preserves the symplectic structure. Distinct from high-fidelity integrators, this paper aims at providing the state transition matrix of a linearized system and ensuring that it preserves the symplectic property that all Hamiltonian systems should possess by nature.

Past studies related to this topic are found in the literature on the Lie-group method and variational integrator [1–3]. It has been shown that these methods provide a systematic way of constructing the structure-preserving numerical integrator by directly discretizing Hamilton's principle rather than the equations of motion. Simo et al. [4] and Kane et al. [5] provide the conditions for the conservation of momentum, energy, and symplecticity in the context of a variational integrator. There is also a class of integrators called symplectic Runge–Kutta methods that preserve the symplectic property while realizing higher-order accuracy [6,7]. Lee et al. [8–10] propose the Lie-group variational integrators, which combines the variational integrator with an exponential map to preserve the Lie-group structure and successfully applies this to rigid-body dynamics under gravitational attraction. In contrast with these studies, this paper focuses on linearized Hamiltonian systems and derives the numerical method for generating the symplectic transition matrix. Distinct from existing symplectic integrators, which provide the state-vector-to-state-vector mapping between different times, the scheme derived in this paper provides the mapping between a whole range of linear solution spaces between two different times. Although it seems obvious that a state transition matrix such as this is derivable from the symplectic integrator schemes, it does not necessarily mean that its derivation and resulting performance are straightforward and trivial, as will be seen in the following sections. To clarify the terminology, we denote SSTM as the symplectic state transition matrix induced physically from a Hamiltonian system, and we denote numerical SSTM as the numerical method of deriving the state transition matrix that preserves symplecticity in this paper.

On the other hand, the state transition matrix of the orbital dynamics problem is widely studied. Recently, many methods of solving the accurate linearized orbital dynamics have been developed, especially through the development of formation-flight technologies, which incorporate perturbation forces either analytically or numerically. Most of these focus on how precisely the perturbation terms can be incorporated into the state transition matrix [11–15]. Imre and Palmer [16] propose a symplectic and computationally efficient numerical integrator for formation-flying spacecraft under arbitrary perturbation forces, but do not focus on the evaluation of the state transition matrix. A typical example of the importance of the symplectic property for state transition matrices in astrodynamics is found in [17–19], in which it is shown that the propagation of orbit uncertainty has certain constraints and properties that arise from the symplectic form of the state transition matrix. Thus, it is important to maintain these properties when mapping orbit uncertainty.

Received 24 November 2008; accepted for publication 17 April 2009.

*Assistant Professor, Institute of Space and Astronautical Science, Department of Space Systems and Astronautics, 3-1-1 Yoshinodai, Sagamihara. Member AIAA.

†A. Richard Seebass Endowed Chair Professor, Mail Code 429 UCB. Member AIAA.

This paper describes the solution-space mapping scheme of linearized Hamiltonian systems and derives the numerical SSTM with an arbitrary order of precision. The Hamiltonian that can be implemented with this scheme includes linearized dynamics with time-varying, nonperiodic coefficients, for which a general solution can be obtained only by means of numerical integration. Because it is applicable to any canonical Hamiltonian system (most of the problems on nondissipative orbital mechanics fall into this category), it can accommodate not only the gravity of the primary body, but also the geopotential terms to any order and third-body perturbations, when applied to the orbital dynamics problem. It can be expected that this scheme can be applied to, for example, the accurate, yet computationally efficient, dynamic filters, long-term formation-flight dynamics, and eigenstructure/manifold studies of the N-body dynamics.

II. Basic Properties of the Symplectic State Transition Matrix

In this section, we will derive some basic properties of the SSTM that are indispensable for later discussions. Although most of the properties here are well-known results for Hamiltonian systems, we attempt to explain them in light of the state transition matrix.

A. Hamiltonian System and Symplectic State Transition Matrix

Let us start from a Lagrangian with the general potential $U(\mathbf{q}, t)$:

$$L(\mathbf{q}, \dot{\mathbf{q}}, t) = \tfrac{1}{2}\dot{\mathbf{q}}^{\mathbf{T}}\dot{\mathbf{q}} - U(\mathbf{q}, t) \tag{1}$$

where $\mathbf{q}$ and t are the generalized coordinates and time, respectively. This Lagrangian form is quadratic in terms of velocity. It will be shown in Sec. VI that a more general Lagrangian (with nonquadratic terms) can also be considered. Hamilton's principle requires the action integral, which is the path integral of the Lagrangian along a time-parameterized trajectory, to be stationary; that is,

$$\delta I = \int_{t_0}^{t_f} \delta L(\mathbf{q}, \dot{\mathbf{q}}, t)\mathrm{d}t = 0 \tag{2}$$

Solving Eq. (2) results in obtaining the Euler-Lagrange equations. If we introduce a generalized momentum $\mathbf{p}$, defined by

$$\mathbf{p} = \frac{\partial}{\partial \dot{\mathbf{q}}} L(\mathbf{q}, \dot{\mathbf{q}}, t) \tag{3}$$

it provides a relationship between $\mathbf{p}$ and $L(\mathbf{q}, \dot{\mathbf{q}}, t)$ and leads to Hamilton $H(\mathbf{q}, \mathbf{p}, t) = \mathbf{p}\dot{\mathbf{q}} - L(\mathbf{q}, \dot{\mathbf{q}}, t)$. Thus, we obtain the Hamilton

$$\dot{\mathbf{q}} = \frac{\partial H}{\partial \mathbf{p}}, \qquad \dot{\mathbf{p}} = -\frac{\partial H}{\partial \mathbf{q}} \tag{4}$$

or, in the compact form,

$$\dot{\boldsymbol{\eta}} = \mathbf{J}\frac{\partial H(\boldsymbol{\eta}, t)}{\partial \boldsymbol{\eta}}, \qquad \boldsymbol{\eta} = \begin{bmatrix} \mathbf{q} \\ \mathbf{p} \end{bmatrix}, \qquad \mathbf{J} = \begin{bmatrix} \mathbf{0} & \mathbf{1} \\ -\mathbf{1} & \mathbf{0} \end{bmatrix} \tag{5}$$

where $\mathbf{p}$ and $\mathbf{q}$ are n-dimensional vectors and $\mathbf{0}$ and $\mathbf{1}$ are the $n \times n$ null and identity matrix, respectively. Note that the $2n \times 2n$ matrix $\mathbf{J}$ has the following special properties:

$$\mathbf{J}^2 = -\mathbf{1}, \qquad \mathbf{J}^T\mathbf{J} = \mathbf{1}, \qquad \mathbf{J}^T = -\mathbf{J}, \qquad |\mathbf{J}| = 1 \tag{6}$$

Now consider the linearization of the system equation (5) around nominal solution $\boldsymbol{\eta} = \boldsymbol{\eta}_0$. The linearized equation becomes

$$\delta\dot{\boldsymbol{\eta}} = \mathbf{J}\left.\frac{\partial^2 H(\boldsymbol{\eta}, t)}{\partial \boldsymbol{\eta}^2}\right|_{\boldsymbol{\eta}=\boldsymbol{\eta}_0} \bullet \delta\boldsymbol{\eta} \tag{7}$$

where we define a small variation from the nominal trajectory by $\boldsymbol{\eta} = \boldsymbol{\eta}_0 + \delta\boldsymbol{\eta}$. If we denote $\boldsymbol{\Phi}(t, t_0)$ as the state transition matrix for Eq. (7), it satisfies

$$\dot{\boldsymbol{\Phi}}(t, t_0) = \mathbf{J}\left.\frac{\partial^2 H(\boldsymbol{\eta}, t)}{\partial \boldsymbol{\eta}^2}\right|_{\boldsymbol{\eta}=\boldsymbol{\eta}_0} \bullet \boldsymbol{\Phi}(t, t_0) \tag{8}$$

The state transition matrix $\boldsymbol{\Phi}(t, t_0)$ is known to be a symplectic matrix (i.e., one that satisfies the relation):

$$\boldsymbol{\Phi}^T\mathbf{J}\boldsymbol{\Phi} = \mathbf{J} \tag{9}$$

Indeed, this can be easily proven by letting $\boldsymbol{\Xi} = \boldsymbol{\Phi}^T\mathbf{J}\boldsymbol{\Phi}$ and differentiating it with respect to t. Taking into account the relations in Eq. (6), we get

$$\dot{\boldsymbol{\Xi}} = \dot{\boldsymbol{\Phi}}^T\mathbf{J}\boldsymbol{\Phi} + \boldsymbol{\Phi}^T\mathbf{J}\dot{\boldsymbol{\Phi}} = \boldsymbol{\Phi}^T\left(\frac{\partial^2 H(\boldsymbol{\eta}_0, t)}{\partial \boldsymbol{\eta}^2}\right)^T\mathbf{J}^T\mathbf{J}\boldsymbol{\Phi} + \boldsymbol{\Phi}^T\mathbf{J}\mathbf{J}\frac{\partial^2 H(\boldsymbol{\eta}_0, t)}{\partial \boldsymbol{\eta}^2}\boldsymbol{\Phi} = \mathbf{0} \tag{10}$$

As $\boldsymbol{\Phi}(t_0, t_0)^T\mathbf{J}\boldsymbol{\Phi}(t_0, t_0) = \mathbf{J}$, we obtain Eq. (9).

If we split the $2n \times 2n$ symplectic matrix into four $n \times n$ submatrices

$$\boldsymbol{\Phi} = \begin{bmatrix} \mathbf{A} & \mathbf{B} \\ \mathbf{C} & \mathbf{D} \end{bmatrix} \tag{11}$$

the equality equation (9) is equivalent to

$$\mathbf{A}^T\mathbf{D} - \mathbf{C}^T\mathbf{B} = \mathbf{1}, \qquad \mathbf{A}^T\mathbf{C} = \mathbf{C}^T\mathbf{A}, \qquad \mathbf{D}^T\mathbf{B} = \mathbf{B}^T\mathbf{D} \tag{12}$$

which can be used as an alternative condition for a matrix to be symplectic.

It can easily be derived from Eqs. (6) and (9) that if $\boldsymbol{\Phi}_1$ and $\boldsymbol{\Phi}_2$ are symplectic, then $\boldsymbol{\Phi}_1\boldsymbol{\Phi}_2$ is also symplectic. Also, we can get the following symplectic inverse formula from these equations:

$$\boldsymbol{\Phi}^{-1} = \mathbf{J}^{-1}\boldsymbol{\Phi}^T\mathbf{J} = -\mathbf{J}\boldsymbol{\Phi}^T\mathbf{J} \tag{13}$$

These properties are important mathematical structures and show that the symplectic matrices form a group. They are also useful for practical numerical computations when using SSTM.

B. Eigenstructure of the Symplectic Matrix

Let λ and $\boldsymbol{\mu}$ denote the eigenvalue and eigenvector of the state transition matrix $\boldsymbol{\Phi}$, respectively. They satisfy

$$\boldsymbol{\Phi}\boldsymbol{\mu} = \lambda\boldsymbol{\mu} \tag{14}$$

Hence,

$$\boldsymbol{\mu}^T\boldsymbol{\Phi}^T = \lambda\boldsymbol{\mu}^T$$

$$\Rightarrow \lambda\boldsymbol{\mu}^T\mathbf{J}\boldsymbol{\Phi} = \boldsymbol{\mu}^T\boldsymbol{\Phi}^T\mathbf{J}\boldsymbol{\Phi} = \boldsymbol{\mu}^T\mathbf{J}$$

and consequently,

$$(\boldsymbol{\mu}^T\mathbf{J})\boldsymbol{\Phi} = \lambda^{-1}(\boldsymbol{\mu}^T\mathbf{J}) \tag{15}$$

where $\boldsymbol{\mu}^T\mathbf{J}$ and λ^{-1} are seen to be the left eigenvector and eigenvalue of $\boldsymbol{\Phi}$, respectively. Therefore, if $\boldsymbol{\Phi}$ is a real matrix, and if one of the eigenvalues is λ, then λ^{-1}, $\bar{\lambda}$, and $\bar{\lambda}^{-1}$ are also eigenvalues of $\boldsymbol{\Phi}$, where we denote $\bar{\lambda}$ as the conjugate of λ.

Also from this property, the following relation can be obtained:

$$\det\boldsymbol{\Phi} = \prod_i \lambda_i = 1 \tag{16}$$

C. Symplectic Transformation

The symplectic property shown so far is valid only when we choose Hamiltonian coordinates $(\mathbf{q}, \mathbf{p})$. However, it can be generalized to arbitrary Lagrangian coordinates $(\mathbf{q}, \dot{\mathbf{q}})$, which

expands the applicability of the SSTM to Hamiltonian systems written in non-Hamiltonian coordinates.

Let $\boldsymbol{\eta}$ denote the Hamiltonian coordinates, and let $\boldsymbol{\xi}$ denote Lagrangian coordinates related to $\boldsymbol{\eta}$. Then let the state transition matrices from $\boldsymbol{\eta}(t_1)$ to $\boldsymbol{\eta}(t_2)$ and from $\boldsymbol{\xi}(t_1)$ to $\boldsymbol{\xi}(t_2)$ be denoted by $\boldsymbol{\Phi}(t_2, t_1)$ and $\boldsymbol{\Psi}(t_2, t_1)$, respectively. Hence,

$$\begin{aligned}\boldsymbol{\Psi}(t_2,t_1) &= \frac{\partial \boldsymbol{\xi}(t_2)}{\partial \boldsymbol{\xi}(t_1)} = \frac{\partial \boldsymbol{\xi}(t_2)}{\partial \boldsymbol{\eta}(t_2)} \cdot \frac{\partial \boldsymbol{\eta}(t_2)}{\partial \boldsymbol{\eta}(t_1)} \cdot \frac{\partial \boldsymbol{\eta}(t_1)}{\partial \boldsymbol{\xi}(t_1)} \\ &= \mathbf{P}(t_2)^{-1} \cdot \boldsymbol{\Phi}(t_2,t_1) \cdot \mathbf{P}(t_1) \end{aligned} \tag{17}$$

where

$$\mathbf{P}(t) \triangleq \frac{\partial \boldsymbol{\eta}(t)}{\partial \boldsymbol{\xi}(t)}, \qquad \frac{\partial \boldsymbol{\eta}(t_2)}{\partial \boldsymbol{\eta}(t_1)} \triangleq \boldsymbol{\Phi}(t_2,t_1), \qquad \frac{\partial \boldsymbol{\xi}(t_2)}{\partial \boldsymbol{\xi}(t_1)} \triangleq \boldsymbol{\Psi}(t_2,t_1)$$

Therefore, from Eqs. (9) and (17), $\boldsymbol{\Psi}(t_2, t_1)$ is found to satisfy

$$\boldsymbol{\Psi}(t_2,t_1)^T \mathbf{P}(t_2)^T \mathbf{J} \mathbf{P}(t_2) \boldsymbol{\Psi}(t_2,t_1) = \mathbf{P}(t_1)^T \mathbf{J} \mathbf{P}(t_1) \tag{18}$$

This is called the symplectic transformation. The symplectic transformation changes the basis, represented by the matrix $\mathbf{P}(t)$, such that

$$\mathbf{J} \mapsto \mathbf{P}(t)^T \mathbf{J} \mathbf{P}(t) \tag{19}$$

Note that the new basis may be a function of time. Because of this, the group property holds only for state transition matrices with consecutive times; that is, the symplectic property Eq. (18) for $\boldsymbol{\Psi}(t_4, t_3)\boldsymbol{\Psi}(t_2, t_1)$ is preserved only when $t_3 = t_2$. Equation (13), which is valid for a symplectic matrix satisfying Eq. (9), has its correspondence for a symplectic-transformed matrix satisfying Eq. (18); that is,

$$\boldsymbol{\Psi}(t_2,t_1)^{-1} = (\mathbf{P}(t_1)^T \mathbf{J} \mathbf{P}(t_1))^{-1} \boldsymbol{\Psi}(t_2,t_1)^T (\mathbf{P}(t_2)^T \mathbf{J} \mathbf{P}(t_2)) \tag{20}$$

If $\mathbf{P}$ is a constant matrix, there is no such limitation on the time. This situation arises in many problems such as, for example, the restricted three-body problem, the Earth orbiter problem, and many other practical situations.

III. Derivation of the Numerical Computation Scheme for the Symplectic State Transition Matrix

A. Discretization of Hamiltonian Dynamics

Consider discretizing the process equations (1–3). The discrete Lagrangian corresponding to Eq. (1) can be written in the following form:

$$\begin{aligned} L_k(\mathbf{q}_k, \mathbf{q}_{k+1}, t_k, t_{k+1}) &= \alpha h L\left(\mathbf{q}_k, \frac{\mathbf{q}_{k+1}-\mathbf{q}_k}{h}, t_k\right) \\ &+ (1-\alpha) h L\left(\mathbf{q}_{k+1}, \frac{\mathbf{q}_{k+1}-\mathbf{q}_k}{h}, t_{k+1}\right) \end{aligned} \tag{21}$$

where h is a step size defined by $h = t_{k+1} - t_k$, and $\alpha \in [0, 1]$ is a parameter of the discretization. The condition for the action integral Eq. (2) yields

$$\delta I = \sum_k \delta L_k = \sum_k \left[\frac{1}{h}(\mathbf{q}_k - \mathbf{q}_{k-1}) - \frac{1}{h}(\mathbf{q}_{k+1} - \mathbf{q}_k) - h\frac{\partial U_k}{\partial \mathbf{q}_k}\right]^T \cdot \delta \mathbf{q}_k = 0 \tag{22}$$

where we define $U_k = U(\mathbf{q}_k, t_k)$, for simplicity. On the other hand, the discretization of Eq. (3) provides the following two equalities:

$$\begin{aligned} \mathbf{p}_k &= -\frac{\partial}{\partial \mathbf{q}_k} L_k(\mathbf{q}_{k+1}, \mathbf{q}_k, t_k, t_{k+1}) = \frac{1}{h}(\mathbf{q}_{k+1} - \mathbf{q}_k) + \alpha h \frac{\partial U_k}{\partial \mathbf{q}_k} \\ \mathbf{p}_{k+1} &= \frac{\partial}{\partial \mathbf{q}_{k+1}} L_k(\mathbf{q}_{k+1}, \mathbf{q}_k, t_k, t_{k+1}) = \frac{1}{h}(\mathbf{q}_{k+1} - \mathbf{q}_k) \\ &- (1-\alpha) h \frac{\partial U_{k+1}}{\partial \mathbf{q}_{k+1}} \end{aligned} \tag{23}$$

Hence, from Eqs. (22) and (23), we obtain

$$\begin{aligned} \mathbf{q}_{k+1} &= \mathbf{q}_k + h\mathbf{p}_k - \alpha h^2 \frac{\partial U_k}{\partial \mathbf{q}_k} \\ \mathbf{p}_{k+1} &= \mathbf{p}_k - \alpha h \frac{\partial U_k}{\partial \mathbf{q}_k} - (1-\alpha) h \frac{\partial U_{k+1}}{\partial \mathbf{q}_{k+1}} \end{aligned} \tag{24}$$

If the potential function is linearized as

$$\frac{\partial U(\mathbf{q}, t)}{\partial \mathbf{q}} = \frac{\partial U(\mathbf{q}_0, t)}{\partial \mathbf{q}} + \frac{\partial^2 U(\mathbf{q}_0, t)}{\partial \mathbf{q}^2} \Delta \mathbf{q} \tag{25}$$

then Eq. (24) can be written in matrix form as

$$\begin{bmatrix} \Delta \mathbf{q}_{k+1} \\ \Delta \mathbf{p}_{k+1} \end{bmatrix} = \mathbf{F}_k \cdot \begin{bmatrix} \Delta \mathbf{q}_k \\ \Delta \mathbf{p}_k \end{bmatrix}$$

$$\mathbf{F}_k = \begin{bmatrix} \mathbf{1} - \alpha h^2 \frac{\partial^2 U_k}{\partial \mathbf{q}_k^2} & h\mathbf{1} \\ -\alpha h \frac{\partial^2 U_k}{\partial \mathbf{q}_k^2} - (1-\alpha) h \frac{\partial^2 U_{k+1}}{\partial \mathbf{q}_{k+1}^2} \left(\mathbf{1} - \alpha h^2 \frac{\partial^2 U_k}{\partial \mathbf{q}_k^2}\right) & \mathbf{1} - (1-\alpha) h^2 \frac{\partial^2 U_{k+1}}{\partial \mathbf{q}_{k+1}^2} \end{bmatrix} \tag{26}$$

where $\Delta \mathbf{q}_k$, $\Delta \mathbf{p}_k$ are the variations of $\mathbf{q}_k$ and $\mathbf{p}_k$. In Eq. (26), $\mathbf{F}_k$ is the discrete mapping from k to $k + 1$.

B. Condition for Symplecticity

If we apply Eq. (12) to the discrete mapping $\mathbf{F}_k$ in Eq. (26), $\mathbf{F}_k$ is formed to be symplectic only when

$$\alpha = 0, \qquad \alpha = 1, \quad \text{or} \quad \frac{\partial^2 U_k}{\partial \mathbf{q}_k^2} \frac{\partial^2 U_{k+1}}{\partial \mathbf{q}_{k+1}^2} = \frac{\partial^2 U_{k+1}}{\partial \mathbf{q}_{k+1}^2} \frac{\partial^2 U_k}{\partial \mathbf{q}_k^2} \tag{27}$$

where $\alpha = 0$ corresponds to the backward differential, and $\alpha = 1$ corresponds to the forward differential, both of which have only first-order accuracy. The third condition in Eq. (27) does not hold true for arbitrary potential functions.

On the other hand, second-order accuracy can be realized when the midpoint-rule is adopted:

$$\alpha = \tfrac{1}{2} \tag{28}$$

Therefore, second-order accuracy and symplecticity do not coexist by simply using Eq. (26). One of the possible realizations of the discrete mapping, which has both second-order and symplectic properties, is to split the sequence into two parts, first applying $\alpha = 0$ and then applying $\alpha = 1$,

$$\begin{bmatrix} \Delta \mathbf{q}_{k+1/2} \\ \Delta \mathbf{p}_{k+1/2} \end{bmatrix} = \begin{bmatrix} \mathbf{1} & h\mathbf{1} \\ -h \frac{\partial^2 U_{k+1/2}}{\partial \mathbf{q}_{k+1/2}^2} & \mathbf{1} - h^2 \frac{\partial^2 U_{k+1/2}}{\partial \mathbf{q}_{k+1/2}^2} \end{bmatrix} \begin{bmatrix} \Delta \mathbf{q}_k \\ \Delta \mathbf{p}_k \end{bmatrix} \quad \text{and}$$

$$\begin{bmatrix} \Delta \mathbf{q}_{k+1} \\ \Delta \mathbf{p}_{k+1} \end{bmatrix} = \begin{bmatrix} \mathbf{1} - h^2 \frac{\partial^2 U_{k+1/2}}{\partial \mathbf{q}_{k+1/2}^2} & h\mathbf{1} \\ -h \frac{\partial^2 U_{k+1/2}}{\partial \mathbf{q}_{k+1/2}^2} & \mathbf{1} \end{bmatrix} \begin{bmatrix} \Delta \mathbf{q}_{k+1/2} \\ \Delta \mathbf{p}_{k+1/2} \end{bmatrix} \tag{29}$$

which can be shown to have second-order accuracy by

$$\begin{aligned} f(x+h) &= f\left(x + \frac{h}{2}\right) + \frac{\partial f(x + (h/2))}{\partial x} \frac{h}{2} = f(x) \\ &+ \frac{\partial f(x + (h/2))}{\partial x} h \approx f(x) + \frac{\partial f(x)}{\partial x} h + \frac{1}{2} \frac{\partial^2 f(x)}{\partial x^2} h^2 \end{aligned}$$

Conversely, we can first apply $\alpha = 1$ and then $\alpha = 0$,

$$\begin{bmatrix} \Delta\mathbf{q}_{k+1/2} \\ \Delta\mathbf{p}_{k+1/2} \end{bmatrix} = \begin{bmatrix} \mathbf{1} - h^2 \frac{\partial^2 U_k}{\partial \mathbf{q}_k^2} & h\mathbf{1} \\ -h \frac{\partial^2 U_k}{\partial \mathbf{q}_k^2} & \mathbf{1} \end{bmatrix} \begin{bmatrix} \Delta\mathbf{q}_k \\ \Delta\mathbf{p}_k \end{bmatrix} \quad \text{and}$$

$$\begin{bmatrix} \Delta\mathbf{q}_{k+1} \\ \Delta\mathbf{p}_{k+1} \end{bmatrix} = \begin{bmatrix} \mathbf{1} & h\mathbf{1} \\ -h \frac{\partial^2 U_{k+1}}{\partial \mathbf{q}_{k+1}^2} & \mathbf{1} - h^2 \frac{\partial^2 U_{k+1}}{\partial \mathbf{q}_{k+1}^2} \end{bmatrix} \begin{bmatrix} \Delta\mathbf{q}_{k+1/2} \\ \Delta\mathbf{p}_{k+1/2} \end{bmatrix} \tag{30}$$

which can also be shown to have second-order accuracy by

$$f(x+h) = f\left(x + \frac{h}{2}\right) + \frac{\partial f(x+h)}{\partial x}\frac{h}{2} = f(x) + \frac{\partial f(x)}{\partial x}\frac{h}{2} + \frac{\partial f(x+h)}{\partial x}\frac{h}{2} \approx f(x) + \frac{\partial f(x)}{\partial x}h + \frac{1}{2}\frac{\partial^2 f(x)}{\partial x^2}h^2$$

As a consequence, the discrete state mapping

$$\mathbf{\Phi}_{k+1} = \mathbf{F}_k \mathbf{\Phi}_k \tag{31}$$

is symplectic and has second-order accuracy at the same time when we choose

$$\mathbf{F}_k = \begin{bmatrix} \mathbf{1} - \left(\frac{h}{2}\right)^2 \frac{\partial^2 U_{k+1/2}}{\partial \mathbf{q}_{k+1/2}^2} & \frac{h}{2}\mathbf{1} \\ -\frac{h}{2}\frac{\partial^2 U_{k+1/2}}{\partial \mathbf{q}_{k+1/2}^2} & \mathbf{1} \end{bmatrix} \begin{bmatrix} \mathbf{1} & h\mathbf{1} \\ -\frac{h}{2}\frac{\partial^2 U_{k+1/2}}{\partial \mathbf{q}_{k+1/2}^2} & \mathbf{1} - \left(\frac{h}{2}\right)^2 \frac{\partial^2 U_{k+1/2}}{\partial \mathbf{q}_{k+1/2}^2} \end{bmatrix} = \begin{bmatrix} \mathbf{1} - \frac{h^2}{2}\frac{\partial^2 U_{k+1/2}}{\partial \mathbf{q}_{k+1/2}^2} & h(\mathbf{1} - \frac{h^2}{4}\frac{\partial^2 U_{k+1/2}}{\partial \mathbf{q}_{k+1/2}^2}) \\ -h\frac{\partial^2 U_{k+1/2}}{\partial \mathbf{q}_{k+1/2}^2} & \mathbf{1} - \frac{h^2}{2}\frac{\partial^2 U_{k+1/2}}{\partial \mathbf{q}_{k+1/2}^2} \end{bmatrix} \tag{32}$$

or

$$\mathbf{F}_k = \begin{bmatrix} \mathbf{1} & \frac{h}{2}\mathbf{1} \\ -\frac{h}{2}\frac{\partial^2 U_{k+1}}{\partial \mathbf{q}_{k+1}^2} & \mathbf{1} - \left(\frac{h}{2}\right)^2 \frac{\partial^2 U_{k+1}}{\partial \mathbf{q}_{k+1}^2} \end{bmatrix} \begin{bmatrix} \mathbf{1} - \left(\frac{h}{2}\right)^2 \frac{\partial^2 U_k}{\partial \mathbf{q}_k^2} & \frac{h}{2}\mathbf{1} \\ -\frac{h}{2}\frac{\partial^2 U_k}{\partial \mathbf{q}_k^2} & \mathbf{1} \end{bmatrix} = \begin{bmatrix} \mathbf{1} - \frac{h^2}{2}\frac{\partial^2 U_k}{\partial \mathbf{q}_k^2} & h\mathbf{1} \\ -\frac{h}{2}\frac{\partial^2 U_{k+1}}{\partial \mathbf{q}_{k+1}^2} - \frac{h}{2}\frac{\partial^2 U_k}{\partial \mathbf{q}_k^2} + \frac{h^3}{4}\frac{\partial^2 U_{k+1}}{\partial \mathbf{q}_{k+1}^2}\frac{\partial^2 U_k}{\partial \mathbf{q}_k^2} & \mathbf{1} - \frac{h^2}{2}\frac{\partial^2 U_{k+1}}{\partial \mathbf{q}_{k+1}^2} \end{bmatrix} \tag{33}$$

Now we denote that $\mathbf{F}_k$ is a second-order-accurate numerical symplectic state transition matrix (numerical SSTM). The elements of $\mathbf{F}_k$ in Eqs. (32) and (33) can be concretely calculated, as all the parameters in the matrix (i.e., $\mathbf{q}_k$, $\mathbf{q}_{k+1}$) are given by the a priori reference orbit information.

C. Relation to Symplectic Integration

The second-order numerical SSTM [Eqs. (32) and (33)] are tightly related to the theory of symplectic integration [20]. Let $\hat{H}$ denote the Lie operator associated with the Hamiltonian H (Hamiltonian operator), defined as

$$\frac{d}{dt}\begin{pmatrix} \mathbf{q} \\ \mathbf{p} \end{pmatrix} = \dot{\boldsymbol{\eta}} = \hat{H} \cdot \boldsymbol{\eta} = \{\boldsymbol{\eta}, H(\boldsymbol{\eta})\} = \sum_i \left(\frac{\partial \boldsymbol{\eta}}{\partial q_i}\frac{\partial H}{\partial p_i} - \frac{\partial \boldsymbol{\eta}}{\partial p_i}\frac{\partial H}{\partial q_i}\right) \tag{34}$$

where $\{\bullet, \bullet\}$ is the Poisson bracket. The solution for Eq. (34) can be decomposed in the following two ways:

$$\boldsymbol{\eta}(t) = \exp(h\hat{H}(t)) \cdot \boldsymbol{\eta}(0) = \exp(h\hat{K} + h\hat{U}(t)) \cdot \boldsymbol{\eta}(0) \approx \exp\left(\frac{h}{2}\hat{K}\right)\exp\left(h\hat{U}\left(t + \frac{h}{2}\right)\right)\exp\left(\frac{h}{2}\hat{K}\right) \cdot \boldsymbol{\eta}(0) + \mathcal{O}(h^3) \tag{35a}$$

$$\boldsymbol{\eta}(t) \approx \exp\left(\frac{h}{2}\hat{U}(t+h)\right)\exp(h\hat{K})\exp\left(\frac{h}{2}\hat{U}(t)\right) \cdot \boldsymbol{\eta}(0) + \mathcal{O}(h^3) \tag{35b}$$

where $\hat{K}$ and $\hat{U}$ are the Lie operators associated with the kinetic energy and potential, respectively, which satisfy $H = K + U$. Note that Eqs. (35a) and (35b) use the same decomposition method of the exponential functions (the Zassenhaus formula), just replacing the roles of $\hat{K}$ and $\hat{U}$. Imposing that the system is linear, we obtain the matrix expressions for the kinetic energy and potential operators:

$$\exp(h\hat{K}) = \begin{pmatrix} \mathbf{1} & h\mathbf{1} \\ \mathbf{0} & \mathbf{1} \end{pmatrix}, \qquad \exp(h\hat{U}(t)) = \begin{pmatrix} \mathbf{1} & \mathbf{0} \\ -h\frac{\partial^2 U(\mathbf{q},t)}{\partial \mathbf{q}^2} & \mathbf{1} \end{pmatrix} \tag{36}$$

Substituting Eq. (36) into Eq. (35), the first approximation equation (35a) yields

$$\exp\left(\frac{h}{2}\hat{K}\right)\exp(h\hat{U}(t_{k+1/2}))\exp\left(\frac{h}{2}\hat{K}\right) = \begin{bmatrix} \mathbf{1} - \frac{h^2}{2}\frac{\partial^2 U_{k+1/2}}{\partial \mathbf{q}_{k+1/2}^2} & h\left(\mathbf{1} - \frac{h^2}{4}\frac{\partial^2 U_{k+1/2}}{\partial \mathbf{q}_{k+1/2}^2}\right) \\ -h\frac{\partial^2 U_{k+1/2}}{\partial \mathbf{q}_{k+1/2}^2} & \mathbf{1} - \frac{h^2}{2}\frac{\partial^2 U_{k+1/2}}{\partial \mathbf{q}_{k+1/2}^2} \end{bmatrix} \tag{37}$$

and Eq. (35b) yields

$$\exp\left(\frac{h}{2}\hat{U}(t_{k+1})\right)\exp(h\hat{K})\exp\left(\frac{h}{2}\hat{U}(t_k)\right) = \begin{bmatrix} \mathbf{1} - \frac{h^2}{2}\frac{\partial^2 U_k}{\partial \mathbf{q}_k^2} & h\mathbf{1} \\ -\frac{h}{2}\frac{\partial^2 U_{k+1}}{\partial \mathbf{q}_{k+1}^2} - \frac{h}{2}\frac{\partial^2 U_k}{\partial \mathbf{q}_k^2} + \frac{h^3}{4}\frac{\partial^2 U_{k+1}}{\partial \mathbf{q}_{k+1}^2}\frac{\partial^2 U_k}{\partial \mathbf{q}_k^2} & \mathbf{1} - \frac{h^2}{2}\frac{\partial^2 U_{k+1}}{\partial \mathbf{q}_{k+1}^2} \end{bmatrix} \tag{38}$$

which are both identical to the results in Eqs. (32) and (33).

Because both the kinetic energy and potential operators in Eq. (36) are symplectic, it is evident that the state transition matrix equations (37) and (38) are also symplectic. Also evident from Eqs. (37) and (38), the numerical SSTM derived here is symmetric in time, which means that this numerical SSTM is time-reversible.

D. Higher-Order Symplectic State Transition Matrix

As a natural extension of the concept used in symplectic integration, a symplectic state transition matrix with higher-order accuracy can be obtained by decomposing the Hamiltonian operator to an arbitrary order. Although there are numerous ways of decomposing the Hamiltonian operator [21–23], let us provide the two typical decompositions, which are known as *fractal decomposition* :

$$\mathbf{S}_m(h,t) = \mathbf{S}_{m-1}(s_m h, t + (1-s_m)h)\mathbf{S}_{m-1}((1-2s_m)h, t + s_m h)\mathbf{S}_{m-1}(s_m h, t)$$

$$\mathbf{S}_2(h,t) = \exp\left(\frac{h}{2}\hat{K}\right)\exp\left(h\hat{U}\left(t + \frac{h}{2}\right)\right)\exp\left(\frac{h}{2}\hat{K}\right) \quad \text{with} \quad s_m = \frac{1}{2 - \sqrt[m]{2}} \tag{39}$$

and

$$\mathbf{S}'_m(h,t) = \mathbf{S}'_{m-1}(s'_m h, t + (1-s'_m)h)\mathbf{S}'_{m-1} \times (s'_m h, t + (1-2s'_m)h)\mathbf{S}'_{m-1}((1-4s'_m)h, t + 2s'_m h) \times \mathbf{S}'_{m-1}(s'_m h, t + s'_m h)\mathbf{S}'_{m-1}(s'_m h, t)$$

$$\mathbf{S}'_2(h,t) = \exp\left(\frac{h}{2}\hat{K}\right)\exp\left(h\hat{U}\left(t + \frac{h}{2}\right)\right)\exp\left(\frac{h}{2}\hat{K}\right) \quad \text{with} \quad s'_m = \frac{1}{4 - \sqrt[m]{4}} \tag{40}$$

Note that numerical SSTM defined by Eq. (39) or Eq. (40) is still time-reversible. In the preceding equations, both Eqs. (37) and (38) can actually be used as a definition of $S_2(h,t)$ and $S_2'(h,t)$, but hereafter, Eq. (37) is exclusively used, because the variation of the potential function appears only once per operator in Eq. (37), whereas in Eq. (38), it appears twice.

Now, instead of Eq. (35), consider the following 3-stage and 5-stage fractal decompositions of the exponential operator induced from Eqs. (39) and (40), respectively:

For the 3-stage decomposition [by Eq. (39)],

$$\mathbf{S}_3(h,t) = \mathbf{S}_2(s_3 h, t + (1-s_3)h) \times \mathbf{S}_2((1-2s_3)h, t + s_3 h)\mathbf{S}_2(s_3 h, t) \quad \text{with} \quad s_3 = \frac{1}{2 - \sqrt[3]{2}} \tag{41}$$

For the 5-stage decomposition [by Eq. (40)],

$$\mathbf{S}_3'(h,t) = \mathbf{S}_2'(s_3' h, t + (1-s_3)h)\mathbf{S}_2'(s_3' h, t + (1-2s_3')h) \times \mathbf{S}_2'((1-4s_3')h, t + 2s_3' h)\mathbf{S}_2'(s_3' h, t + s_3' h)\mathbf{S}_2'(s_3' h, t) \quad \text{with} \quad s_3' = \frac{1}{4 - \sqrt[3]{4}} \tag{42}$$

Although the proof is omitted, Eq. (41) has third-order accuracy with respect to h, and Eq. (42) has fourth-order accuracy [24,25]. The full detail of each element in Eq. (41) is provided in Appendix A. It is also possible to obtain an even-higher-order numerical SSTM by recursively applying Eq. (39) or Eq. (40).

IV. Performance Evaluation

A. Integration Step Size and Accuracy

To evaluate the characteristics of the numerical SSTM, the following six combinations of state transition matrix and integration schemes are prepared:

EUL is the linear state transition matrix and Euler integration scheme. RK4 is the linear state transition matrix and fourth-order Runge–Kutta integration scheme. RK45 is the linear state transition matrix and fifth-order adaptive step-size Runge–Kutta integration scheme. SYMP1 is the second-order 1-stage numerical SSTM [Eq. (37)] and discrete mapping scheme [Eq. (31)]. SYMP3 is the third-order 3-stage numerical SSTM [Eq. (41)] and discrete mapping scheme [Eq. (31)]. SYMP5 is the fourth-order 5-stage numerical SSTM [Eq. (42)] and discrete mapping scheme [Eq. (31)].

These integration schemes are tested with various integration step sizes (divisions/orbital revolution) using the conditions shown in Table 1. We employ the simple two-body dynamics for this benchmark evaluation; that is,

$$U = -\frac{\mu}{r} \tag{43}$$

Figure 1 shows the integration error after 10 orbital revolutions. The upper 3 figures in Fig. 1 are the result for the low Earth orbit (LEO) (case a in Table 1), and the lower 3 figures are for the elliptic orbit

The symplecticity, energy error, and position error are evaluated by the following equations:

$$\text{symplecticity} = |\mathbf{\Phi}(t,0)^T \mathbf{J} \mathbf{\Phi}(t,0) - \mathbf{J}|, \quad \text{where } |\mathbf{X}| = \sqrt{\text{tr}(\mathbf{X}^T \mathbf{X})} \tag{44}$$

$$\text{energy error} = \frac{E(t) - E_{\text{real}}}{E_{\text{real}}} \tag{45}$$

$$\text{position error} = \frac{\Delta \mathbf{r}(t) - \Delta \mathbf{r}_{\text{real}}(t)}{\Delta r_{\text{real}}(0)} \tag{46}$$

where $E(t)$, $\Delta\mathbf{r}(t)$ are the orbital energy and the relative position of the follower satellite, obtained from each state transition matrix integration scheme, and E_{real} and $\Delta\mathbf{r}_{\text{real}}(t)$ are those calculated by a high-precision orbit propagator (two-body dynamics without any approximations). Note that the energy error and position error are normalized by the constant initial values E_{real} and $\Delta r_{\text{real}}(0)$.

The symplecticity is well satisfied with any higher-order symplectic schemes, but performs poorly for SYMP1 (analogous to the EUL approach), except at small step sizes. RK4 can achieve a low symplecticity error only when a very small step size is selected. RK4 and SYMP5 can express the actual energy the best for case a, but those advantages vanish in case b, and RK4, SYMP1, SYMP3, and SYMP5 show almost the same performance with regard to the energy.

The most notable point here is that, as can be expected from the formulation, the symplectic state transition matrix holds an almost even level of the geometrical structure-preserving property, regardless of the integration step size. This leads us to justify the use of some special characteristics that the symplectic matrix has, such as the structure-preserving property and the matrix inverse property [Eq. (13)]. The variable step-size integrator RK45 can achieve better accuracy than RK4, especially for case b. However, even with RK45, we cannot obtain the highly accurate symplectic property as we do with the symplectic schemes.

Figure 2 shows the integration accuracy of SYMP3 with various step sizes, in which case a in Table 1 is used for the calculation conditions. It can be said that a smaller step size gives better results for the positional accuracy. The symplectic error and energy error do not necessarily decrease as a smaller step size is employed. This is because if we employ a smaller step size, it requires a larger number of matrix-product operations, which increases the truncation error. This implies that there is an optimum step size to best preserve the symplectic structure. However, even for a large step size, the symplecticity and energy error are not so much deteriorated, but rather bounded for as long as hundreds of revolutions, even though the positional accuracy is affected strongly by the step size. This bounded property for energy (with oscillation near the true value) is exactly what we can observe by general symplectic integrators ([2]).

B. Eccentricity and Integration Accuracy

Figure 3 shows the integration accuracy performance of SYMP3, evaluated with the orbital eccentricity as a parameter. The apogee is parameterized in Fig. 3 to realize various eccentricities, and the other calculation conditions are based on Table 1, with a 500 div/rev (division/revolution) step size (constant step size).

Table 1 Conditions for performance evaluations

	Case a: circular orbit	Case b: high-eccentricity orbit
Reference orbit		
Orbital model	Two-body dynamics	Two-body dynamics
Perigee altitude	500 km	500 km
Apogee altitude	500 km	36000 km
Eccentricity (derived)	0.0	0.72
Leader satellite	On reference orbit	On reference orbit
Follower satellite	100 m radial offset along the semimajor axis (orbital period identical to leader)	
Evaluation period	100 rev (∼6.6 days)	100 rev (∼44.5 days)

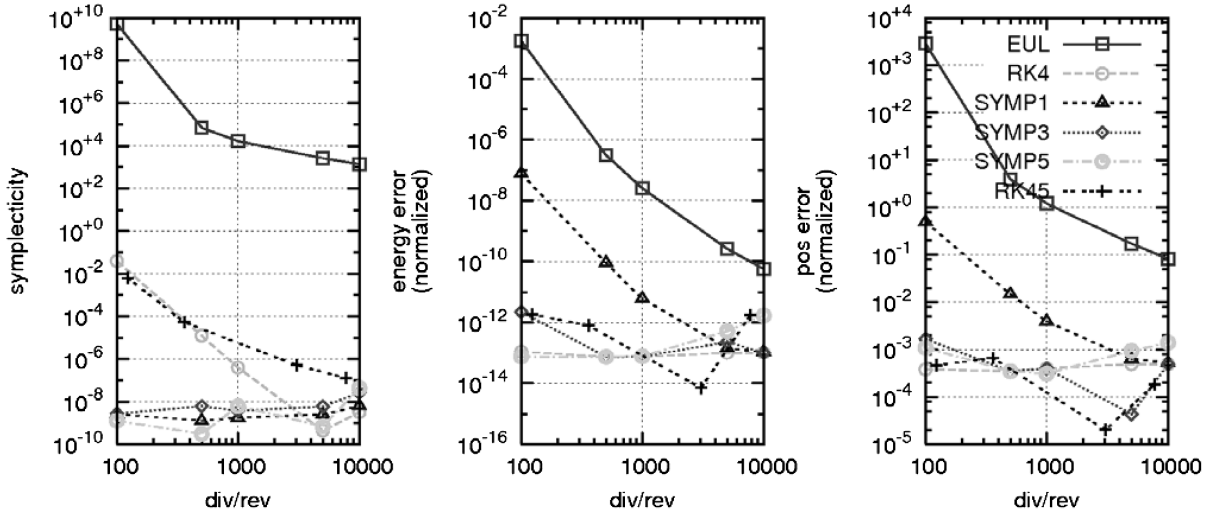

Case (a): 500km LEO Orbit (e=0.0)

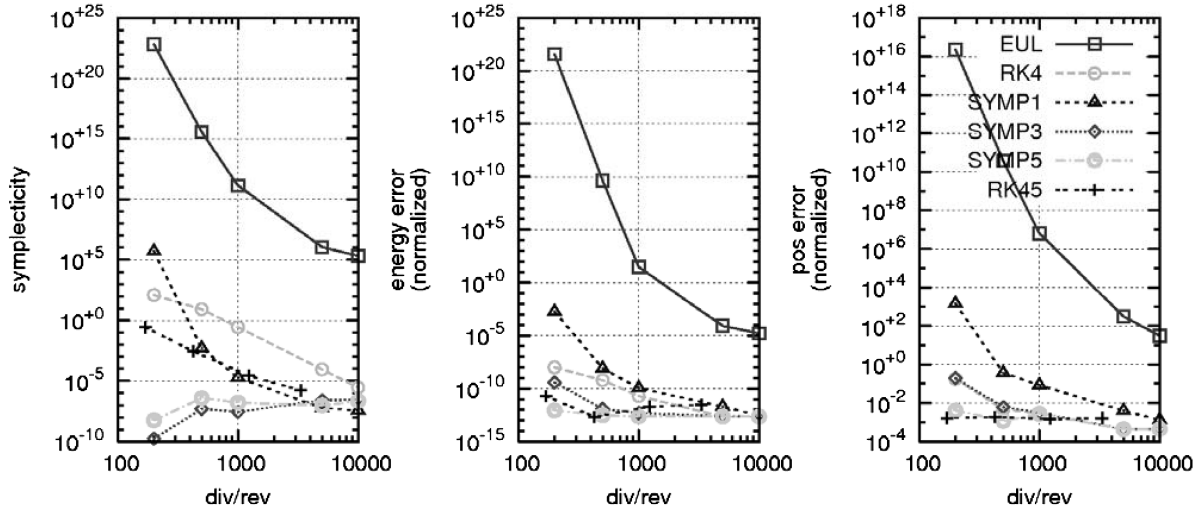

Case (b): 500km by 36000km Elliptic Orbit (e=0.72)

Fig. 1 Step size and integration accuracy for various linear mapping schemes. The horizontal axes are in divisions per revolution which is related to the step size h and the orbital period T by $\mathrm{div/rev} = T/h$. The average step size is used for RK45. The same definition is used for the subsequent figures.

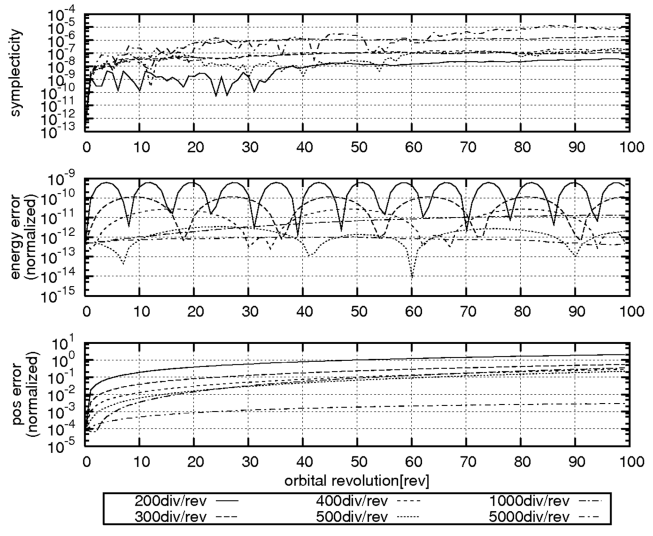

Fig. 2 Integration accuracy of SYMP3 with various integration step sizes.

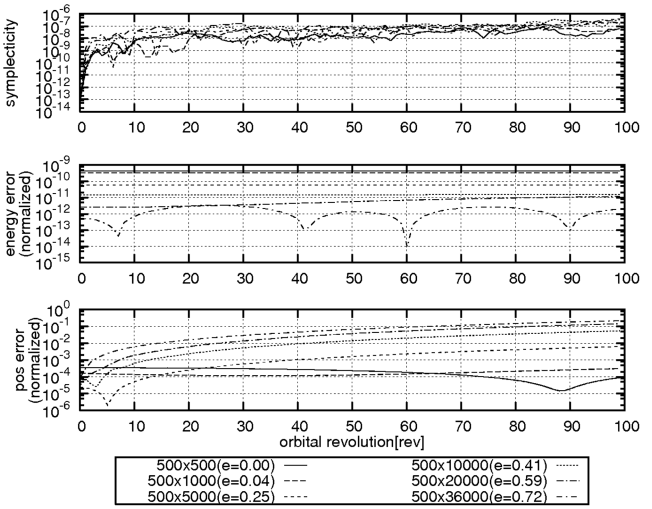

Fig. 3 Integration accuracy of SYMP3 with various eccentricity.

When compared at the same integration step size, a smaller eccentricity provides a better positional accuracy. As to the symplecticity and energy error, all the cases give similar accuracy for a long duration.

C. Integration Accuracy and Computational Cost

Figure 4 compares the integration accuracy performance of each linear mapping scheme for case a in Table 1, with the step-size set to give identical computational times for each routine. This comparison most clearly shows the advantages of the numerical SSTM scheme. They are summarized as follows:

1) For symplecticity, SYMP1, SYMP3, and SYMP5 are the best and comparable.

2) For energy conservation, RK4, SYMP3, and SYMP5 are the best and comparable.

3) For positional error, RK4, SYMP3, and SYMP5 are the best and comparable.

4) All the symplectic schemes attain very low symplecticity error, which cannot be obtained by EUL nor RK4.

5) RK4, SYMP3, and SYMP5 achieve the best results in view of energy error and position error, but SYMP3 and SYMP5 attain more accurate symplecticity in addition, with looser (larger) integration step sizes.

6) SYMP5 does not increase the accuracy as compared with SYMP3.

V. Eigenstructure-Preserving Performance of Numerical SSTM

A. Determinant Characteristics

As the numerical SSTM is guaranteed to preserve the symplectic structure, it is expected to preserve the determinant characteristics equation (16) automatically. There are no such characteristics expected for the linear state transition matrix computed with the conventional integration schemes such as Euler and Runge–Kutta integrations.

Figures 5 and 6 show simulation examples of the determinant error (deviation from 1) of the state transition matrix, calculated along LEO (case a in Table 1) and high-eccentricity orbit (case b), using EUL, RK4, SYMP1, SYMP3, and SYMP5. The determinant errors of SYMP2, SYMP3, and SYMP5 are very low, whereas those for EUL and RK4 are relatively high. It can also be seen that as long as we choose a sufficient step size to maintain numerical stability, the determinant error is kept low even after the long integration.

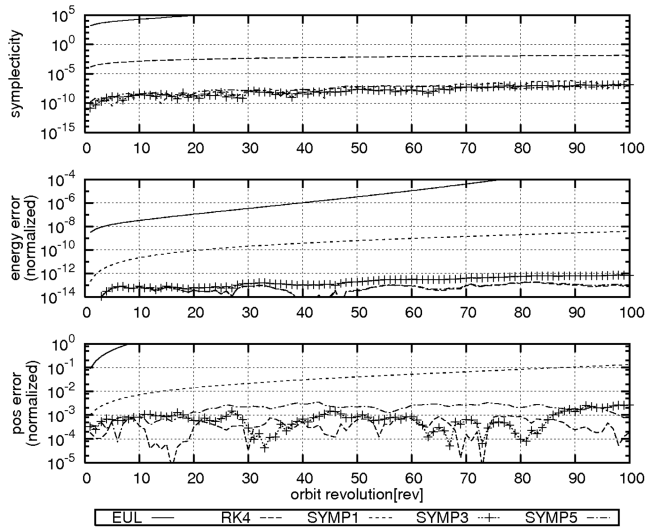

Fig. 4 Integration accuracy of various linear mapping schemes compared at the identical computational time (EUL:936 div/rev, RK4:196 div/rev, SYMP1:722 div/rev, SYMP3:210 div/rev, and SYMP5:131 div/rev).

B. Eigenvalues Distributions

To study the eigenvalue distribution properties of the state transition matrix for numerical SSTM, we restrict ourselves to the Keplerian dynamics case in this section, as the general case is much more difficult. Then the Hamiltonian system can be expressed as

$$H = \frac{1}{2}\dot{\mathbf{p}}\cdot\dot{\mathbf{p}} + U(\mathbf{q}), \qquad \dot{\mathbf{q}} = \frac{\partial H}{\partial \mathbf{p}}, \qquad \dot{\mathbf{p}} = -\frac{\partial H}{\partial \mathbf{q}} \tag{47}$$

The precise potential gradient can be written in the form

$$\begin{aligned}\frac{\partial U}{\partial \mathbf{q}} &= \frac{\partial U}{\partial \mathbf{q}_0} + \frac{\partial^2 U}{\partial \mathbf{q}_0^2}\Delta\mathbf{q} + \mathcal{O}(\Delta\mathbf{q}^2)\\ &\triangleq \frac{\partial U}{\partial \mathbf{q}_0} + \left(\frac{\partial^2 U}{\partial \mathbf{q}_0^2} + \boldsymbol{\varepsilon}(\mathbf{q}_0, \Delta\mathbf{q})\right)\Delta\mathbf{q}\end{aligned} \tag{48}$$

where $\boldsymbol{\varepsilon}(\mathbf{q}_0, \Delta\mathbf{q})$ represents the residual of the approximation and can be interpreted as the spatial variation of the linearization error of the potential gradient. The resulting linearized equation for the Hamiltonian system equation (47) becomes

$$\frac{d}{dt}\begin{bmatrix}\Delta\mathbf{q}\\ \Delta\mathbf{p}\end{bmatrix} = \begin{bmatrix}\mathbf{0} & \mathbf{1}\\ -\frac{\partial^2 U}{\partial \mathbf{q}^2} - \boldsymbol{\varepsilon}(\mathbf{q}_0, \Delta\mathbf{q}) & \mathbf{0}\end{bmatrix}\begin{bmatrix}\Delta\mathbf{q}\\ \Delta\mathbf{p}\end{bmatrix} \tag{49}$$

If we consider the potential for the Keplerian dynamics equation (43), and if $\boldsymbol{\varepsilon}(\mathbf{q}_0, \Delta\mathbf{q})$ is set to zero, the state transition matrix over one orbital period (monodromy matrix) in rotational coordinates is known to take the following form [14]:

$$\boldsymbol{\Phi}((n+1)T, nT) = e^{\boldsymbol{\Lambda}T} = \begin{bmatrix} 1 & & & & & \\ -w_{21} & 1 & & & -w_{25} & \\ & & 1 & & & \\ -w_{41} & & & 1 & -w_{45} & \\ & & & & 1 & \\ & & & & & 1 \end{bmatrix} \triangleq \mathbf{1}^{(6)} - \boldsymbol{\Pi} \tag{50}$$

where n is an arbitrary integer, T is the orbital period, $\mathbf{1}^{(6)}$ is the 6×6 identity matrix,

$$w_{21} = \frac{6(1+e)(2+e)\pi}{(-1+e)^2\sqrt{1-e^2}}, \qquad w_{25} = \frac{6(1+e)^2\pi}{(-1+e)^2\sqrt{1-e^2}}\frac{1}{\dot{\theta}}$$

$$w_{41} = \frac{6e(2+e)\pi}{(-1+e)^2\sqrt{1-e^2}}\dot{\theta}, \qquad w_{45} = \frac{6e(1+e)\pi}{(-1+e)^2\sqrt{1-e^2}}$$

$$\dot{\theta} = \frac{\sqrt{\mu/a^3}(1+e\cos\theta)^2}{(1-e^2)^{3/2}}$$

It is easily obtained from Eq. (50) that

$$\boldsymbol{\Lambda}\, T = -\boldsymbol{\Pi} \tag{51}$$

On the other hand, if we do not neglect $\boldsymbol{\varepsilon}(\mathbf{q}_0, \Delta\mathbf{q})$, it can be proved that the monodromy matrix takes the following form (for the proof, see Appendix B):

$$\boldsymbol{\Phi}'((n+1)T, nT) = e^{\boldsymbol{\Lambda}T + \Delta\boldsymbol{\Lambda}(nT)T}$$

$$= \exp\begin{bmatrix} 0 & 0 & 0 & 0 & 0 & 0\\ -w_{21} & 0 & 0 & 0 & -w_{25} & 0\\ 0 & 0 & 0 & 0 & 0 & 0\\ -w_{41} - T\varepsilon_{11} & -T\varepsilon_{12} & -T\varepsilon_{13} & 0 & -w_{45} & 0\\ -T\varepsilon_{21} & -T\varepsilon_{22} & -T\varepsilon_{23} & 0 & 0 & 0\\ -T\varepsilon_{31} & -T\varepsilon_{32} & -T\varepsilon_{33} & 0 & 0 & 0 \end{bmatrix} \tag{52}$$

The eigenvalues of $\boldsymbol{\Phi}'((n+1)T, nT)$ can now be calculated concretely by Eq. (52). They are

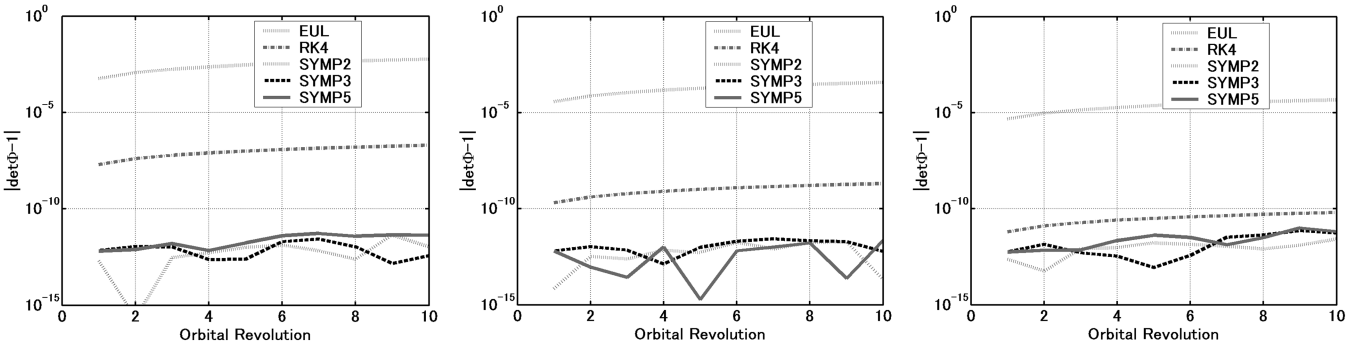

Fig. 5 Determinant error for 10 rev in 500 km LEO (left: 200, middle: 500, and right: 1000 div/rev).

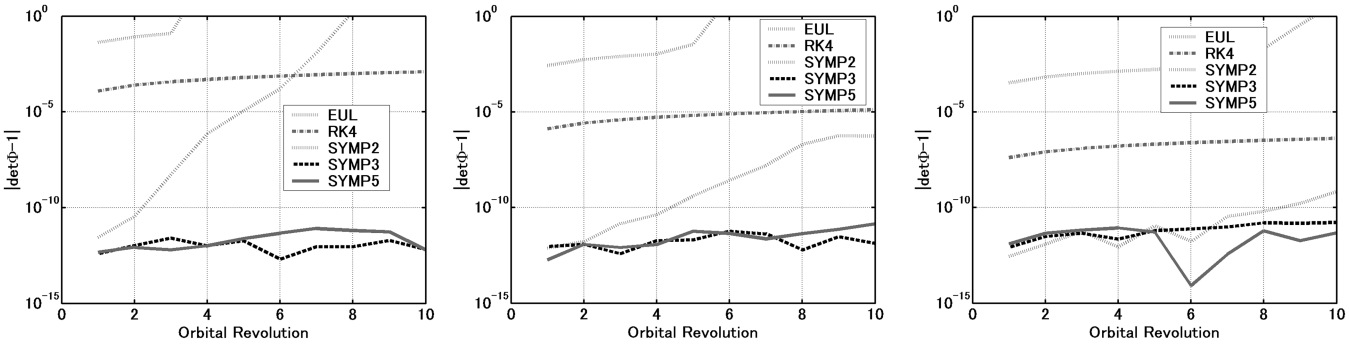

Fig. 6 Determinant error for 10 rev in 500 × 36, 000 km high elliptic orbit (left: 200, middle: 500, and right: 1000 div/rev).

$$\lambda_i(\boldsymbol{\Phi}'((n+1)T, nT)) = 1, 1, 1, 1, e^{-\sqrt{p_{25}T\varepsilon_{22}}}, e^{\sqrt{p_{25}T\varepsilon_{22}}} \tag{53}$$

The preceding eigenvalues are independent of the selection of the coordinate system (i.e., valid for both the rotational coordinates and inertial coordinates), as the coordinate transformation does not affect the eigenvalues and eigenvectors in general.

Equation (53) reveals that the eigenvalues of the precise state transition matrix without error all have unit magnitude. However, if there is a small error due to the linearization of the potential, two out of the six eigenvalue magnitudes deviate from 1.

The magnitude of the error $\boldsymbol{\varepsilon}$ is expected to depend on two quantities. First, it depends on the magnitude of the nonlinear term. This cannot be controlled as long as we deal with a linearized system. Second, it depends on the precision of the integration scheme (i.e., the order of the integration). Concerning the integration schemes dealt with in this paper, therefore, the order of precision is anticipated to be EUL < SYMP2 < SYMP3 < RK4 ≅ SYMP5.

Figures 7 and 8 show the eigenvalues distributions of the state transition matrices generated by each integration scheme. The figures plot the eigenvalues of the state transition matrix at one orbital period step up to 10 rev. The eigenvalue distributions indicate that the two eigenvalues deviate from 1 along the unit circle as the revolution number increases, which implies that $w_{25}\varepsilon_{22} < 0$ in these cases. It can also be seen that among SYMP3, RK4 and SYMP5 or RK4 and SYMP5 are the best (SYMP5 is slightly better than RK4), as is expected from the order of the integration schemes.

Consequently, it can be said that the precision of each eigenvalue depends on the linearization error and the order of the integration scheme. Specifically, two of the eigenvalues can easily deviate from 1, and this is inevitable even when we employ symplectic schemes, as the state transition matrix provides only the linear state mapping and it cannot compensate for nonlinear terms. Nevertheless, the numerical SSTM can precisely preserve the symplectic structure and determinant characteristics that the state transition matrix should have, which cannot be realized with a conventionally computed linear state transition matrix.

VI. Numerical SSTM for the Circular Restricted Three-Body Problem

The symplectic state transition matrix derived in this paper can also be applied to the circular restricted three-body problem (CRTBP). The state transition matrix expressed in the libration point-fixed (rotational) coordinates, which is the one chosen for CRTBP formulations, is not symplectic with the basis **J**. But it can always be

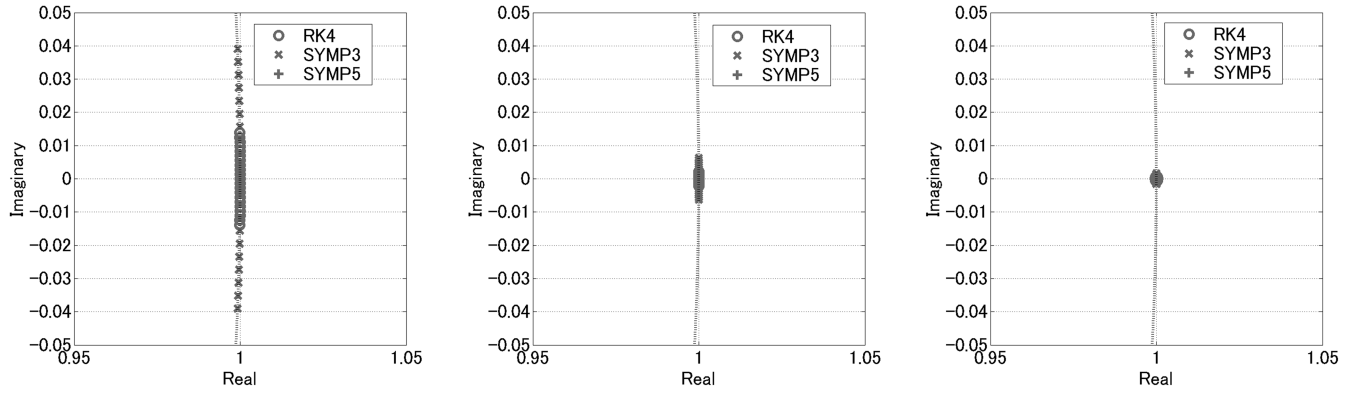

Fig. 7 Eigenvalues distributions for 10 rev in 500 km LEO (left: 200, middle: 500, right: 1000 div/rev, and dotted curve represents the unit circle).

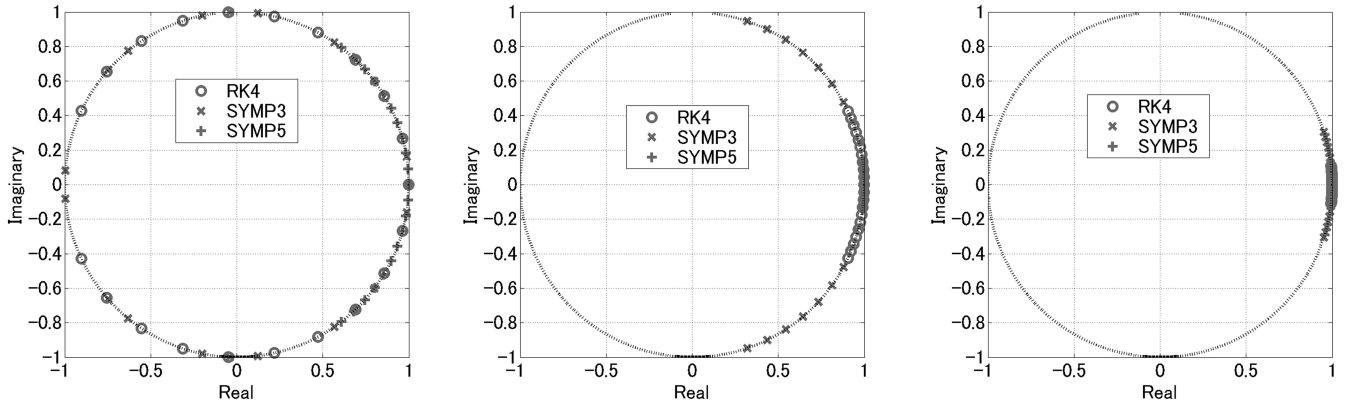

Fig. 8 Eigenvalues distributions for 10 rev in 500 × 36, 000 km High elliptic orbit. (left: 200, middle: 500, right: 1000 div/rev, dotted curve represents the unit circle).

transformed to coordinates that fit within the Hamiltonian formalism. As any Hamiltonian system holds the symplectic property, we can show that the state transition matrix for CRTBP has a symplectic structure with a different basis. In the same sense, it can be shown that the symplectic state transition matrix derived so far can be extended and applied to the CRTBP, which enjoys a structure-preserving property similar to the numerical SSTM shown in the previous sections.

A. Geometrical Structure of CRTBP

The equations of motion for the CRTBP, expressed in a libration point-fixed rotating coordinate system, are written as [26]

$$\ddot{x} - 2\dot{y} = -\frac{\partial U^*}{\partial x}, \qquad \ddot{y} + 2\dot{x} = -\frac{\partial U^*}{\partial y}, \qquad \ddot{z} = -\frac{\partial U^*}{\partial z} \tag{54}$$

with the pseudopotential

$$U^* = -\frac{1}{2}(x^2 + y^2) + U = -\frac{1}{2}(x^2 + y^2) - \frac{(1-\nu)(x - X_1)}{|\mathbf{r} - \mathbf{R}_1|} - \frac{\nu(x - X_2)}{|\mathbf{r} - \mathbf{R}_2|} \tag{55}$$

where $\mathbf{r} = (xyz)^T$ is the position vector expressed in the rotating coordinates, $\mathbf{R}_i = (X_i Y_i Z_i)^T$ $(i = 1, 2)$ are the positions of the primary body (P1) and secondary body (P2), and $\nu = m_2/(m_1 + m_2)$ is the mass ratio induced from the P1 mass m_1 and P2 mass m_2. The variables here are normalized with the semimajor axis, lengthwise, and mean motion of P2 about P1, timewise (i.e., $a = 1$ and $n = 1$).

The Lagrangian of the system equation (54) can be written as

$$L = K - U = \tfrac{1}{2}(\mathbf{v} + \boldsymbol{\omega} \times \mathbf{r})^2 - U \tag{56}$$

where K is the kinetic energy, and $\mathbf{v} + \boldsymbol{\omega} \times \mathbf{r}$ is the velocity in the inertial frame (with $\boldsymbol{\omega} = (0, 0, 1)^T$.)

To fit to the Hamiltonian formalism, one can apply the coordinate transformation from $\boldsymbol{\xi} = (\mathbf{r}, \mathbf{v})$ to $\boldsymbol{\eta} = (\mathbf{q}, \mathbf{p})$ obtained through Eq. (3):

$$\boldsymbol{\eta} = \begin{pmatrix} q_x \\ q_y \\ q_z \\ p_x \\ p_y \\ p_z \end{pmatrix} = \begin{bmatrix} 1 & 0 & 0 & 0 & 0 & 0 \\ 0 & 1 & 0 & 0 & 0 & 0 \\ 0 & 0 & 1 & 0 & 0 & 0 \\ 0 & -1 & 0 & 1 & 0 & 0 \\ 1 & 0 & 0 & 0 & 1 & 0 \\ 0 & 0 & 0 & 0 & 0 & 1 \end{bmatrix} \begin{pmatrix} x \\ y \\ z \\ v_x \\ v_y \\ v_z \end{pmatrix} \triangleq \mathbf{P}\boldsymbol{\xi} \tag{57}$$

Because $\boldsymbol{\eta}$ are Hamiltonian coordinates, they satisfy Hamilton's equations (4) and (5). Therefore, recalling the discussion in Sec. II.C, the state transition matrix from $\boldsymbol{\eta}(t_1)$ to $\boldsymbol{\eta}(t_2)$ is symplectic, and its symplectic transformation provides the state transition matrix from $\boldsymbol{\xi}(t_1)$ to $\boldsymbol{\xi}(t_2)$.

B. Numerical SSTM for CRTBP

The Lie operator associated with the kinetic energy (kinetic energy operator) is derived via

$$\dot{\boldsymbol{\eta}} = \hat{K} \cdot \boldsymbol{\eta} = \{\boldsymbol{\eta}, K(\boldsymbol{\eta})\} = \sum_i \left(\frac{\partial \boldsymbol{\eta}}{\partial q_i} \frac{\partial K}{\partial p_i} - \frac{\partial \boldsymbol{\eta}}{\partial p_i} \frac{\partial K}{\partial q_i} \right) = \sum_i \left(\frac{\partial \boldsymbol{\eta}}{\partial r_i} \frac{\partial \mathbf{v}}{\partial p_i} \frac{\partial K}{\partial \mathbf{v}} \right) \tag{58}$$

and results in solving Eqs. (54) with their right-hand sides replaced by zeros. Consequently,

$$\exp(h\hat{K}) = \begin{bmatrix} 1 & 0 & 0 & \frac{1}{2}\sin 2h & \frac{1}{2}(1 - \cos 2h) & 0 \\ 0 & 1 & 0 & -\frac{1}{2}(1 - \cos 2h) & \frac{1}{2}\sin 2h & 0 \\ 0 & 0 & 1 & 0 & 0 & h \\ 0 & 0 & 0 & \cos 2h & \sin 2h & 0 \\ 0 & 0 & 0 & -\sin 2h & \cos 2h & 0 \\ 0 & 0 & 0 & 0 & 0 & 1 \end{bmatrix} \tag{59}$$

In the same way, the Lie operator associated with the potential (potential operator) becomes

$$\exp(h\hat{U}^*(t)) = \begin{pmatrix} \mathbf{1} & \mathbf{0} \\ -h\frac{\partial^2 U^*(\mathbf{r})}{\partial \mathbf{r}^2} & \mathbf{1} \end{pmatrix} \tag{60}$$

Note that matrix equations (59) and (60) both form a symplectic group with a constant coordinates transformation matrix $\mathbf{P}$.

The numerical SSTM for the system equation (54) can be derived in the same way as shown in Sec. II, using Eqs. (59) and (60) in place of Eq. (36). The state mapping equation (31) for the system equation (54) preserves the symplectic-transformed structure, as was discussed in Sec. II.C.

C. Numerical Validations

The preceding characteristics are tested numerically for a halo orbit around the sun–Earth L1. The reference orbit is selected as $A_{z0} = 125,000$ km (Fig. 9,) and the orbit of the follower satellite is selected such that it is 1 km apart from the reference orbit at the initial time and is in a different halo orbit.

Figure 10 is the result calculated for 1 orbital period (∼177.5 days) with 100 div/rev. The symplecticity is evaluated using

$$|\mathbf{P}^{-T}\boldsymbol{\Phi}^T\mathbf{P}^T\mathbf{J}\mathbf{P}\boldsymbol{\Phi}\mathbf{P}^{-1} - \mathbf{J}|$$

in place of Eq. (44), and the energy error is evaluated as the difference between the reference orbit's and follower's Hamiltonians using Eq. (45) with the energy replaced by the pseudo energy equation (56). The position error is evaluated based on Eq. (46).

It can be seen from these figures that the numerical SSTMs (SYMP1, SYMP3, and SYMP5) preserve symplecticity better than

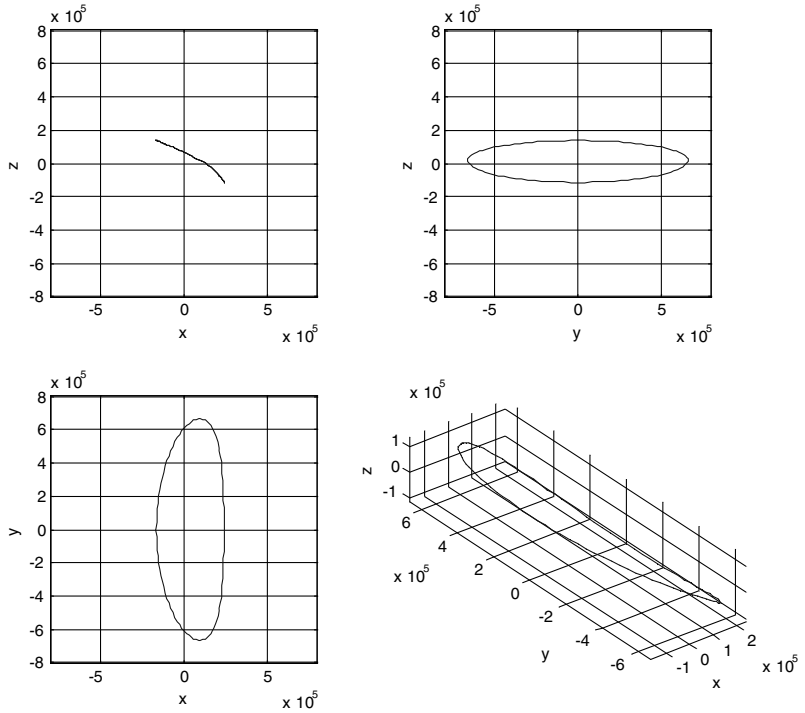

Fig. 9 Halo orbit around sun–Earth L1. $A_{z_0} = 125,000$ km, $a = 1.49598e8$ km, and $n = 1.99099e-7$ rad/s, All axes are in kilometers.

EUL and RK4. They also exhibit the energy-preserving characteristics and position accuracy better than EUL and as good as RK4. By analogy with the discussion in Sec. IV.C, if compared under the same computational time, therefore, the geometry preserving property of the numerical SSTM should be more remarkable.

Different from the two-body problem, the symplecticity and determinant errors are not bounded, showing monotonic increases as time proceeds. This is estimated to be caused, at first, by the truncation error of the numerical SSTM. And then, once a small error is produced, it grows exponentially as time proceeds, due to the unstable eigenvalue in the state transition matrix around the halo orbit. Nevertheless, the symplecticity error in one orbital period is remarkably small when compared with EUL and RK4, and the special characteristic that the geometrical structure conservation property is not dependent on the integration step size holds, as is shown in Sec. IV.A. Furthermore, as the cause of the error is not due to the imperfectness of the formulation but due to the truncation error, it is expected that we can obtain better results by merely applying higher numerical precision variables when implemented into software.

The position errors are relatively large for all the schemes. This is because we calculated the temporary development of the state vector using the state transition matrix (i.e., assuming linear dynamics). Because of the high nonlinearity of the dynamics around halo orbits, it is always insufficient to merely use the state transition matrix to integrate the state vector forward. Nevertheless, the state transition matrix around libration points is important for understanding many aspects of the three-body dynamics study, such as, for example, stable/unstable manifolds, etc., and the numerical SSTM derived in this paper is, by its nature, capable of preserving the geometrical property better.

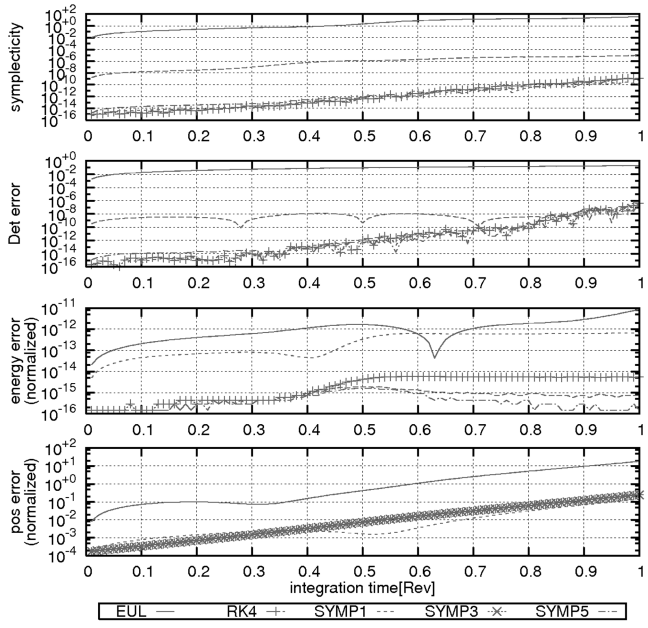

Fig. 10 Integration accuracy of numerical SSTM along a halo orbit.

VII. Numerical SSTM Applied to Real-Ephemeris Simulations

As the third numerical example, we apply our numerical SSTM to an orbit generated with real ephemerides. For the orbit around the Earth, the major terms that we have to consider are the perturbation from the moon, the sun, and the gravitational potential of the Earth. It is also possible to implement the atmospheric drag and solar radiation if needed, but in this case, one cannot expect the state transition matrix to preserve the symplectic property, as it is no longer a Hamiltonian system.

Because the Hamiltonian appearing in the numerical SSTM that we derived can be an explicit function of time, we can implement the perturbation force into the numerical SSTM without changes in the formulations shown in Secs. III and IV. Indeed, we can define the potential function as the explicit function of position and time:

$$U(\mathbf{r},t) = -\frac{\mu}{r} - \left[\sum_{2\le n}\sum_{0\le m<n}\left(\frac{a}{r}\right)^n \bar{P}_{nm}(\sin\phi')(\bar{C}_{nm}\cos m\lambda + \bar{S}_{nm}\sin m\lambda)\right] - \sum_i\left(\frac{\mu_i}{\|\mathbf{r}-\mathbf{R}_i(t)\|} + \frac{\mu_i}{R_i(t)}\right) \tag{61}$$

where the first term of the right-hand side of equation is the point-

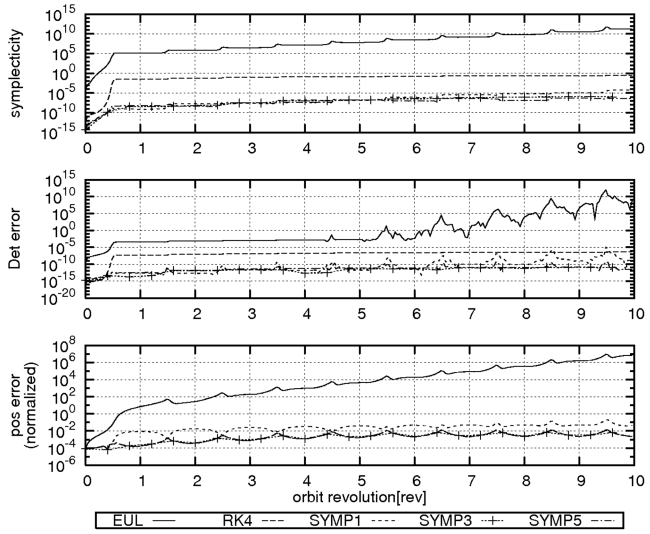

Fig. 11 Integration accuracy of numerical SSTM for real-ephemeris simulation. Calculated for 10 rev starting from 1 January 2010 at 0000 hrs Coordinated Universal Time with the initial state of $(a, e, i, \Omega, \omega, \theta)$= (49, 256 km, 0.72, 30 deg, 0 deg, 0 deg, 180 deg).

mass gravity of the primary body (the Earth), the second term is the higher-order potential of the Earth expressed with the standard notations ($\bar{C}_{nm}$ and $\bar{S}_{nm}$ are normalized gravitational coefficients, λ and ϕ' are the longitude and geodetic latitude of the position $\mathbf{r}$, both of which are the functions of $\mathbf{r}$ and t), and the third term is the effect of the ith celestial body such as the moon and the sun, where μ_i and $\mathbf{R}_i$ are the gravity constant and the position vector of the ith body.

The numerical SSTM can be obtained by calculating the second derivative of U with respect to $\mathbf{r}$ and substituting into Eq. (36) and so on, although this process requires extensive mathematical manipulations.

Figure 11 shows a numerical example of the numerical SSTM using real ephemerides of the moon and the sun. The Earth gravity potential is also implemented up to 10th degree and 10th order ($n = 10$ and $m = 10$). The orbit used for the simulation is an elliptic orbit with 500 km perigee and 36000 km apogee, and the step size of 1000 div/rev is adopted. The other conditions are shown in the figure. It can be seen from the figure that the symplecticity and determinant error are kept quite low for SYMP1, SYMP3, and SYMP5 as compared with EUL and RK4. SYMP3 and SYMP5 achieve positional error as low as RK4, as was the case with the two-body simulations in Sec. IV. Because the real ephemeris is used, energy conservation is not expected in this case.

VIII. Conclusions

This paper presents a numerical method of deriving the symplectic state transition matrix (numerical SSTM) for arbitrary Hamiltonian systems. The numerical SSTM holds the symplectic structure-preserving property and the time-reversible property and can be obtained to an arbitrary order of precision. We derived the numerical SSTM to be applied to Hamiltonian systems with any symplectic basis, with arbitrary potential functions, which can be an explicit function of both time and position. It was also shown both analytically and numerically that the numerical SSTM exhibits better determinant and eigenstructure properties than with the conventional linear state transition matrix with conventional integration schemes such as Euler integration and Runge–Kutta integration. The performance of the numerical SSTM was tested with two-body dynamics, the circular restricted three-body problem, and an Earth orbit subject to perturbation forces based on the real ephemeris of the solar system, all of which reveal the precise structure-preserving property with less computational cost. The numerical SSTM therefore provides accurate discrete state mapping when the structure-preserving property is especially crucial.

Appendix A: Calculation of the 3-Stage Third-Order Numerical SSTM [Eq. (41)]

Note that for implementations for the numerical calculation, one does not need to implement the following equations, but instead, one of Eqs. (39–42) can be used. This Appendix is intended to show how higher-order terms for h (step size) affect the solution-space mapping:

$$\mathbf{S}_3(h,t) = \begin{bmatrix} \mathbf{S}_{11} & \mathbf{S}_{12} \\ \mathbf{S}_{21} & \mathbf{S}_{22} \end{bmatrix} \tag{A1}$$

where $\mathbf{S}_{11}$, $\mathbf{S}_{12}$, $\mathbf{S}_{21}$, and $\mathbf{S}_{22}$ are 3×3 submatrices. Their concrete expressions are

$$\begin{aligned}\mathbf{S}_{11} = \mathbf{1} &- \frac{h^2}{2}[\{3s_3^2 + 2s_3(1-2s_3)\}U_{\mathbf{rr}}(t_1) + \{(1-2s_3)^2 \\ &+ 2s_3(1-2s_3)\}U_{\mathbf{rr}}(t_2) + s_3^2 U_{\mathbf{rr}}(t_3)] + \frac{h^4}{4}[\{s_3(1-2s_3)^3 \\ &+ 3s_3^2(1-2s_3)^2 + 2s_3^3(1-2s_3)\}U_{\mathbf{rr}}(t_2)U_{\mathbf{rr}}(t_1) \\ &+ \{2s_3^3(1-2s_3) + 2s_3^4\}U_{\mathbf{rr}}(t_3)U_{\mathbf{rr}}(t_1) + \{s_3^2(1-2s_3)^2 \\ &+ s_3^3(1-2s_3)\}U_{\mathbf{rr}}(t_3)U_{\mathbf{rr}}(t_2)] - \frac{h^6}{8}[\{s_3^3(1-2s_3)^3 \\ &+ 2s_3^4(1-2s_3)^2 + s_3^5(1-2s_3)\}U_{\mathbf{rr}}(t_3)U_{\mathbf{rr}}(t_2)U_{\mathbf{rr}}(t_1)]\end{aligned} \tag{A2}$$

$$\begin{aligned}\mathbf{S}_{12} = &-\frac{h^3}{4}[\{3s_3^3 + 2s_3^2(1-2s_3)\}U_{\mathbf{rr}}(t_1) + \{(1-2s_3)^3 \\ &+ 4s_3(1-2s_3)^2 + 4s_3^2(1-2s_3)\}U_{\mathbf{rr}}(t_2) + \{3s_3^3 + 2s_3^2 \\ &\times (1-2s_3)\}U_{\mathbf{rr}}(t_3)] + \frac{h^5}{8}[\{s_3(1-2s_3)^2 s_3^3 + 3s_3^3(1-2s_3)^2 \\ &+ 2s_3^4(1-2s_3)\}U_{\mathbf{rr}}(t_2)U_{\mathbf{rr}}(t_1) + \{2s_3^4(1-2s_3) \\ &+ 2s_3^5\}U_{\mathbf{rr}}(t_3)U_{\mathbf{rr}}(t_1) + \{s_3^2(1-2s_3)^3 + 3s_3^3(1-2s_3)^2 \\ &+ 2s_3^4(1-2s_3)\}U_{\mathbf{rr}}(t_3)U_{\mathbf{rr}}(t_2)] - \frac{h^7}{16}[\{s_3^4(1-2s_3)^3 \\ &+ 2s_3^5(1-2s_3)^2 + s_3^6(1-2s_3)\}U_{\mathbf{rr}}(t_3)U_{\mathbf{rr}}(t_2)U_{\mathbf{rr}}(t_1)]\end{aligned} \tag{A3}$$

$$\begin{aligned}\mathbf{S}_{21} = \mathbf{1} &- h[s_3 U_{\mathbf{rr}}(t_1) + (1-2s_3)U_{\mathbf{rr}}(t_2) + s_3 U_{\mathbf{rr}}(t_3)] \\ &+ \frac{h^3}{2}[\{s_3(1-2s_3)^2 + s_3^2(1-2s_3)\}U_{\mathbf{rr}}(t_2)U_{\mathbf{rr}}(t_1) \\ &+ \{2s_3^2(1-2s_3) + 2s_3^3\}U_{\mathbf{rr}}(t_3)U_{\mathbf{rr}}(t_1) + \{s_3(1-2s_3)^2 \\ &+ s_3^2(1-2s_3)\}U_{\mathbf{rr}}(t_3)U_{\mathbf{rr}}(t_2)] - \frac{h^5}{4}[\{s_3^2(1-2s_3)^3 \\ &+ 2s_3^3(1-2s_3)^2 + s_3^4(1-2s_3)\}U_{\mathbf{rr}}(t_3)U_{\mathbf{rr}}(t_2)U_{\mathbf{rr}}(t_1)]\end{aligned} \tag{A4}$$

$$\begin{aligned}\mathbf{S}_{22} = \mathbf{1} &- \frac{h^2}{2}[s_3^2 U_{\mathbf{rr}}(t_1) + \{(1-2s_3)^2 + 2s_3(1-2s_3)\}U_{\mathbf{rr}}(t_2) \\ &+ \{3s_3^2 + 2s_3(1-2s_3)\}U_{\mathbf{rr}}(t_3)] + \frac{h^4}{4}[\{s_3^2(1-2s_3)^2 \\ &+ s_3^3(1-2s_3)\}U_{\mathbf{rr}}(t_2)U_{\mathbf{rr}}(t_1) + \{2s_3^3(1-2s_3) \\ &+ 2s_3^4\}U_{\mathbf{rr}}(t_3)U_{\mathbf{rr}}(t_1) + \{s_3(1-2s_3)^3 + 3s_3^2(1-2s_3)^2 \\ &+ 2s_3^3(1-2s_3)\}U_{\mathbf{rr}}(t_3)U_{\mathbf{rr}}(t_2)] - \frac{h^6}{8}[\{s_3^3(1-2s_3)^3 \\ &+ 2s_3^4(1-2s_3)^2 + s_3^5(1-2s_3)\}U_{\mathbf{rr}}(t_3)U_{\mathbf{rr}}(t_2)U_{\mathbf{rr}}(t_1)]\end{aligned} \tag{A5}$$

where

$$t_1 = t + s_3 h, \qquad t_2 = t + (1 - 2s_3)h, \qquad t_3 = t + (1 - s_3)h$$

$$U_{\mathbf{rr}} = \frac{\partial^2 U}{\partial \mathbf{r}^2} \tag{A6}$$

Note that in Eqs. (A2–A5), the second-order and higher terms of h contribute to satisfy the symplecticity. If we ignore the second and higher terms of h, the conventional linear state transition matrix is obtained, which is nonsymplectic but only consistent.

Appendix B: Proof of Eq. (52)

Suppose $\mathbf{X}_0(t)$ is a fundamental matrix of $\mathbf{x}(t)$ and satisfies the following ordinary differential equation with periodic coefficients:

$$\dot{\mathbf{X}}_0(t) = \mathbf{A}(t)\mathbf{X}_0(t), \qquad \mathbf{X}_0(0) = \mathbf{1}, \qquad \mathbf{A}(t + T) = \mathbf{A}(t) \tag{B1}$$

where T is the period of the coefficients. In the two-body dynamics, T corresponds to the orbital period. From Floquet's theorem, the following characteristic is obtained:

$$\mathbf{X}_0(t + T) = \mathbf{X}_0(t)\mathbf{M}_0 \tag{B2}$$

where $\mathbf{M}_0 = \mathbf{\Phi}((n + 1)T, nT)$ is a constant matrix called the *monodromy matrix*. If we put

$$\mathbf{M}_0 = e^{\mathbf{\Lambda} T} \tag{B3}$$

then the general solution for Eq. (B1) takes the following form:

$$\mathbf{X}_0(t) = \mathbf{F}(t)e^{\mathbf{\Lambda} t}, \qquad \mathbf{F}(t + T) = \mathbf{F}(t) \tag{B4}$$

By substituting Eq. (B4) into Eq. (B1), we get

$$\mathbf{A}(t) = (\dot{\mathbf{F}}(t) + \mathbf{F}(t)\mathbf{\Lambda})\mathbf{F}(t)^{-1}$$

or, equivalently,

$$\mathbf{\Lambda} = \mathbf{F}(t)^{-1}\mathbf{A}(t)\mathbf{F}(t) - \mathbf{F}(t)^{-1}\dot{\mathbf{F}}(t) \tag{B5}$$

Now consider a small nonperiodic term added on the coefficient of the original system (B1),

$$\dot{\mathbf{X}}(t) = (\mathbf{A}(t) + \Delta\mathbf{A}(t))\mathbf{X}(t), \qquad \mathbf{X}(0) = \mathbf{1}$$
$$\mathbf{A}(t + T) = \mathbf{A}(t) \tag{B6}$$

and this can be assumed to cause only small deviations in $\mathbf{\Lambda}$. From Eq. (B5), we get

$$\Delta\mathbf{\Lambda}(t) = \mathbf{F}(t)^{-1}\Delta\mathbf{A}(t)\mathbf{F}(t) \tag{B7}$$

Consequently, the general solution for Eq. (B6) takes the following form:

$$\mathbf{X}(t) = \mathbf{F}(t)e^{(\mathbf{\Lambda} + \Delta\mathbf{\Lambda}(t))t}, \qquad \mathbf{F}(t + T) = \mathbf{F}(t) \tag{B8}$$

The monodromy matrix for Eq. (B8) then becomes

$$\begin{aligned}\mathbf{M}'(n) &= \mathbf{X}(nT)^{-1}\mathbf{X}((n + 1)T) = e^{(\mathbf{\Lambda} + (n+1)\Delta\mathbf{\Lambda}((n+1)T) - n\Delta\mathbf{\Lambda}(nT))T} \\ &= \mathbf{F}(t)^{-1}e^{(\mathbf{F}(t)\mathbf{\Lambda}\mathbf{F}(t)^{-1} + (n+1)\Delta\mathbf{A}((n+1)T) - n\Delta\mathbf{A}(nT))T}\mathbf{F}(t) \\ &\approx \mathbf{F}(t)^{-1}e^{(\mathbf{F}(t)\mathbf{\Lambda}\mathbf{F}(t)^{-1} + \Delta\mathbf{A}(nT))T}\mathbf{F}(t)\end{aligned} \tag{B9}$$

where, in the final transformation, the error growth in one orbital period is assumed to be very slow; that is,

$$\Delta\mathbf{A}((n + 1)T) \approx \Delta\mathbf{A}(nT) + \mathcal{O}(\Delta^2)$$

The monodromy matrix is no longer time-invariant, due to the addition of $\Delta\mathbf{\Lambda}(t)$. As we can put $\mathbf{F}(0) = \mathbf{F}(nT) = \mathbf{1}$ without losing generality, we finally get

$$\mathbf{M}'(n) = \mathbf{\Phi}'((n + 1)T, nT) = e^{\mathbf{\Lambda} T + \Delta\mathbf{A}(t)T} \tag{B10}$$

If we set

$$\Delta\mathbf{\Lambda}(t) = \begin{bmatrix} \mathbf{0} & \mathbf{0} \\ -\boldsymbol{\varepsilon}(t) & \mathbf{0} \end{bmatrix} = \begin{bmatrix} 0 & 0 & 0 & 0 & 0 & 0 \\ 0 & 0 & 0 & 0 & 0 & 0 \\ 0 & 0 & 0 & 0 & 0 & 0 \\ -\varepsilon_{11} & -\varepsilon_{12} & -\varepsilon_{13} & 0 & 0 & 0 \\ -\varepsilon_{21} & -\varepsilon_{22} & -\varepsilon_{23} & 0 & 0 & 0 \\ -\varepsilon_{31} & -\varepsilon_{32} & -\varepsilon_{33} & 0 & 0 & 0 \end{bmatrix} \tag{B11}$$

the desired equality equation (52) is obtained.

References

[1] Hairer, E., Lubich, C., and Wanner, G., *Geometric Numerical Integration*, 2nd ed., Springer–Verlag, New York, 2006.

[2] Marsden, J. E., West, M., "Discrete Mechanics and Variational Integrators," *Acta Numerica*, Vol. 10, Sept. 2001, pp. 357–514. doi:10.1017/S096249290100006X

[3] Iserles, A., Munthe-Kaas, H. Z., Nrsett, S. P., and Zanna, A., "Lie-Group Methods," *Acta Numerica*, Vol. 9, Jan. 2000, pp. 215–365. doi:10.1017/S0962492900002154

[4] Simo, J. C., Tarnow, N., and Wong, K. K., "Exact Energy-Momentum Conserving Algorithms and Symplectic Schemes for Nonlinear Dynamics," *Computer Methods in Applied Mechanics and Engineering*, Vol. 100, No. 1, 1992, pp. 63–116. doi:10.1016/0045-7825(92)90115-Z

[5] Kane, C., Marsden, J. E., and Ortiz, M., "Symplectic-Energy-Momentum Preserving Variational Integrators," *Journal of Mathematical Physics*, Vol. 40, No. 7, 1999, pp. 3353–3371. doi:10.1063/1.532892

[6] Sanz-Serna, J. M., "Runge–Kutta Schemes for Hamiltonian Systems," *BIT*, Vol. 28, No. 4, 1988, pp. 877–883. doi:10.1007/BF01954907

[7] Hu, G., "Symplectic Runge–Kutta Methods for the Kalman-Bucy Filter," *IMA Journal of Mathematical Control and Information*, Vol. 25, No. 2, 2008, pp. 173–183. doi:10.1093/imamci/dnm015

[8] Lee, T., Leok, M., and McClamroch, N. H., "Lie Group Variational Integrators for the Full Body Problem," *Computer Methods in Applied Mechanics and Engineering*, Vol. 196, Nos. 29–30, 2007, pp. 2907–2924. doi:10.1016/j.cma.2007.01.017

[9] Lee, T., Leok, M., and McClamroch, N. H., "Lie Group Variational Integrators for the Full Body Problem in Orbital Mechanics," *Celestial Mechanics and Dynamical Astronomy*, Vol. 98, No. 2, 2007, pp. 121–144. doi:10.1007/s10569-007-9073-x

[10] Lee, T., Leok, M., and McClamroch, N. H., "Discrete Control Systems," *Encyclopedia of Complexity and System Science*, Springer, New York, 2007.

[11] Gim, D. W., and Alfriend, K. T., "The State Transition Matrix for Relative Motion of Formation Flying Satellites," AAS Space Flight Mechanics Meeting, San Antonio, TX, American Astronautical Society Paper 02-186, 2002.

[12] Gim, D.-W., and Alfriend, K. T., "State Transition Matrix of Relative Motion for the Perturbed Non-Circular Reference Orbit," *Journal of Guidance, Control, and Dynamics*, Vol. 26, No. 6, 2003, pp. 956–971. doi:10.2514/2.6924

[13] Ross, M., "Linearized Dynamic Equations for Spacecraft Subject to J2 Perturbations," *Journal of Guidance, Control, and Dynamics*, Vol. 26, No. 4, 2003, pp. 657–659. doi:10.2514/2.5095

[14] Inalhan, G., Tillerson, M., and How, J., "Relative Dynamics and Control of Spacecraft Formations in Eccentric Orbits," *Journal of Guidance, Control, and Dynamics*, Vol. 25, No. 1, 2002, pp. 48–59. doi:10.2514/2.4874

[15] Hamel, J. H., and Lafontaine, J., "Linearized Dynamics of Formation Flying Spacecraft on a J2-Perturbed Elliptical Orbit," *Journal of Guidance, Control, and Dynamics*, Vol. 30, No. 6, 2007, pp. 1649–1658. doi:10.2514/1.29438

[16] Imre, E., and Palmer, L., "High-Precision, Symplectic Numerical, Relative Orbit Propagation," *Journal of Guidance, Control, and Dynamics*, Vol. 30, No. 4, 2007, pp. 965–973. doi:10.2514/1.26846

[17] Hsiao, F. Y., and Scheeres, D. J., "Fundamental Constraints on Uncertainty Evolution in Hamiltonian Systems," *IEEE Transactions on Automatic Control*, Vol. 52, No. 4, 2007, pp. 686–691. doi:10.1109/TAC.2007.894531

[18] Scheeres, D. J., Hsiao, F. Y., Park, R. S., Villac, B. F., and Maruskin, J. M., "Fundamental Limits on Spacecraft Orbit Uncertainty and Distribution Propagation," *Journal of the Astronautical Sciences*, Vol. 54, Nos. 3–4, 2006, pp. 505–523.

[19] Scheeres, D. J., Han, D., and Hou, Y., "Influence of Unstable Manifolds on Orbit Uncertainty," *Journal of Guidance, Control, and Dynamics*, Vol. 24, No. 3, 2001, pp. 573–585. doi:10.2514/2.4749

[20] Kinoshita, H., Yoshida, H., and Nakai, H., "Symplectic Integrators and Their Application in Dynamical Astronomy," *Celestial Mechanics and Dynamical Astronomy*, Vol. 50, No. 1, 1991, pp. 59–71. doi:10.1007/BF00048986

[21] Creutz, M., and Gocksch, A., "High-Order Hybrid Monte Carlo Algorithms," *Physical Review Letters*, Vol. 63, No. 1, 1989, pp. 9–12. doi:10.1103/PhysRevLett.63.9

[22] Forest, E., and Ruth, R. D., "Fourth-Order Symplectic Integrator," *Physica D*, Vol. 43, No. 1, 1990, pp. 105–117. doi:10.1016/0167-2789(90)90019-L

[23] Chin, S. A., "Forward and Nonforward Symplectic Integrators in Solving Classical Dynamics Problems," *International Journal of Computer Mathematics*, Vol. 84, No. 6, 2007, pp. 729–747. doi:10.1080/00207160701458476

[24] Suzuki, M., "Fractal Decomposition of Exponential Operators with Applications to Many-Body Theories and Monte Carlo Simulation," *Physics Letters A*, Vol. 146, No. 6, 1990, pp. 319–323. doi:10.1016/0375-9601(90)90962-N

[25] Yoshida, H., "Construction of High Order Symplectic Integrators," *Physics Letters A*, Vol. 150, Nos. 5–7, 1990, pp. 262–268. doi:10.1016/0375-9601(90)90092-3

[26] Richardson, D. L., "Analytic Construction of Periodic Orbits About the Collinear Points," *Celestial Mechanics*, Vol. 22, No. 3, 1980, pp. 241–253. doi:10.1007/BF01229511